

LOCMAP: LOW-COMPUTE MODEL MERGING WITH AMORTIZED PARETO FRONTS VIA QUADRATIC APPROXIMATION

Anonymous authors

Paper under double-blind review

ABSTRACT

Model merging has emerged as an effective approach to combine multiple single-task models into a multitask model. This process typically involves computing a weighted average of the model parameters without any additional training. Existing model-merging methods focus on enhancing average task accuracy. However, interference and conflicts between the objectives of different tasks can lead to trade-offs during the merging process. In real-world applications, a set of solutions with various trade-offs can be more informative, helping practitioners make decisions based on diverse preferences. In this paper, we introduce a novel and **low-compute algorithm, Model Merging with Amortized Pareto Front (LocMAP)**. LocMAP efficiently identifies a Pareto set of scaling coefficients for merging multiple models, reflecting the trade-offs involved. It amortizes the substantial computational cost of evaluations needed to estimate the Pareto front by using quadratic approximation surrogate models derived from a pre-selected set of scaling coefficients. Experimental results on vision and natural language processing tasks demonstrate that LocMAP can accurately identify the Pareto front, providing practitioners with flexible solutions to balance competing task objectives. We also introduce Bayesian LocMAP for scenarios with a relatively low number of tasks and Nested LocMAP for situations with a high number of tasks, further reducing the computational cost of evaluation.

1 INTRODUCTION

Large pre-trained foundation models have become available in many real-world applications Wornow et al. (2023); Thirunavukarasu et al. (2023); Cui et al. (2024). This increasing availability has led to a popular practice of fine-tuning these pre-trained models to adapt to a wide range of downstream tasks. Practitioners can independently fine-tune the same pre-trained model, such as CLIP style models Radford et al. (2021); Wu et al. (2023); Zhai et al. (2023), large language models Brown et al. (2020); Rozière et al. (2023); Touvron et al. (2023); Jiang et al. (2024), etc., and then release the fine-tuned models without releasing the training data. As the deployment of such fine-tuned models increases, combining models with identical architectures and initializations has emerged as a promising approach to combine their respective capabilities. This is useful, especially in scenarios where the training data for each task is private and cannot be shared, such as individual-level patient data in a hospital and behavior data in social media recommendation systems.

Existing methods for merging models typically involve calculating a weighted average of the parameters from multiple models to enhance performance uniformly across various tasks. However, this approach often overlooks the conflicts among the diverse objectives of these tasks, which can lead to trade-offs in terms of model performance on various tasks. In real-world applications, it is often useful to obtain a set of Pareto optimal solutions rather than a single model. Such solutions allow practitioners to choose among different trade-offs, depending on their specific needs. For example, hospitals specializing in certain areas might prefer a model that excels in tasks relevant to their specialty while maintaining adequate performance across a broader spectrum of diseases.

In this paper, we introduce a novel method that identifies the Pareto front without retraining the models to be merged. Our algorithm utilizes a quadratic approximation of the evaluation metric. Furthermore, we enhance it with a Bayesian adaptive sampling method and a nested merging scheme,

054
055
056
057
058
059
060
061
062
063
064
065
066
067
068
069
070
071
072
073
074
075
076
077
078
079
080
081
082
083
084
085
086
087
088
089
090
091
092
093
094
095
096
097
098
099
100
101
102
103
104
105
106
107

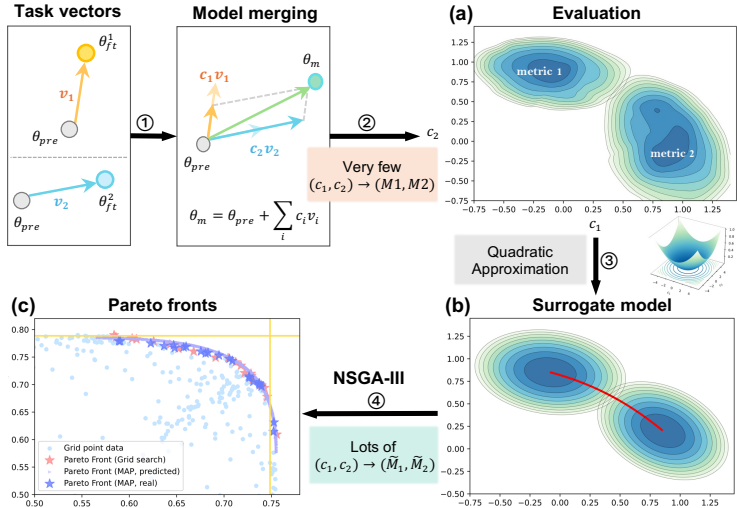


Figure 1: Illustration of the overall process of LocMAP for the case of two tasks. **Step 1:** Select 2 tasks and compute their corresponding task vectors. **Step 2:** Sample a few scaling coefficients c and query the evaluation metrics for each task, respectively. **Step 3:** Use the quadratic model as a surrogate model to approximate the mapping $c \rightarrow \text{metrics}$. **Step 4:** Use the NSGA-III algorithm with the surrogate objective functions to find amortized Pareto fronts. **Subfigure (a)** shows a contour plot of the actual accuracy landscape for the ViT-B/32 model Dosovitskiy et al. (2020) obtained from 100 scaling coefficients (sampled uniformly) evaluated on the SUN397 Xiao et al. (2016) and Cars Krause et al. (2013) datasets. **Subfigure (b)** shows a contour plot of the fitted quadratic functions. Red lines represent the Pareto front in the decision variable (c_1, c_2) space. **Subfigure (c)** shows an example of the resulting Pareto fronts. The Pareto front (Grid search) is regarded as the ground truth given the sufficient number of grid points evaluated. The Pareto front (LocMAP, predicted) is the amortized Pareto front. The Pareto front (LocMAP, real) is the Pareto front involving the same $\{(c_1, c_2)\}$ but re-evaluated to obtain the ground truth metrics for comparison. The yellow lines are the fine-tuned single-task models’ evaluated performance.

which further bring down the computational cost. We validate our method across a diverse set of tasks, spanning from vision to natural language processing, and demonstrate its applicability to a variety of architectures, including ResNets He et al. (2016), ViT Dosovitskiy et al. (2020), and large language models Brown et al. (2020); Rozière et al. (2023); Touvron et al. (2023); Jiang et al. (2024). Our results confirm that this novel approach supports the seamless integration of diverse model capabilities and aligns more closely with various real-world preference by providing a set of optimal fronts across the tasks.

Contributions The main contributions of this paper are:

- C1** We propose the LocMAP algorithm that utilizes quadratic surrogate models to approximate the evaluation metric functions, which amortize the computation of Pareto fronts;
- C2** We demonstrate the effectiveness of LocMAP across a diverse set of architectures, including vision models (e.g., ResNet, ViT) and large language models, showing its generalizability and flexibility for different domains.
- C3** We introduce two variants of LocMAP: the nested-merging LocMAP, which decreases computational complexity from $O(N \cdot 2^N)$ to $O(N \log_2^N)$, and the Bayesian LocMAP, which efficiently queries the computationally expensive evaluations according to loss information.
- C4** To our best knowledge, this paper is the first work, that estimates the Pareto front for task-vector-based model-merging methods with low compute, and without relying on gradient descent for deep neural networks. Our code is available at https://anonymous.4open.science/r/LocMAP_Anonymize.

In Figure 2, we compare our method to direct search. It is important to note that evaluating models in our problem setting is computationally expensive; as a result, our proposed method can only query the

108
109
110
111
112
113
114
115
116
117
118
119
120
121
122
123
124
125
126
127
128
129
130
131
132
133
134
135
136
137
138
139
140
141
142
143
144
145
146
147
148
149
150
151
152
153
154
155
156
157
158
159
160
161

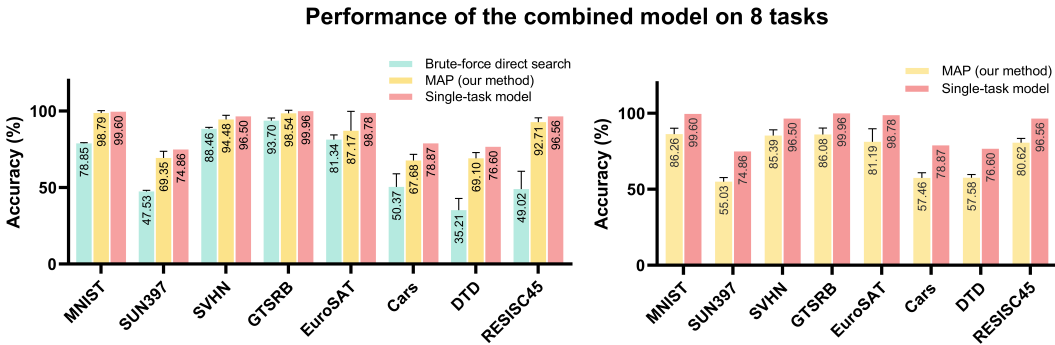


Figure 2: **Subfigure (a)** Comparison of our method with direct search for merged ViT-B/32 models Dosovitskiy et al. (2020), based on evaluation results of 250 combinations of scaling coefficients. Our method identifies a more diverse set of solutions across eight tasks within the same computational budget. Both methods aim to maximize the performance of one task while ensuring that all other tasks meet a minimum threshold of 40%. The bar plot displays the maximized accuracy for each task. **Subfigure (b)** When the threshold is increased to 65% of the single-task model’s performance, the brute-force direct search method fails to find any feasible solutions within the same computational budget.

evaluation pipeline a limited number of times. We choose to compare with direct brute-force search within the scaling coefficient spaces. When the number of tasks is low, the Pareto fronts obtained through direct brute-force search can be considered ground truth because the scaling coefficient spaces have been sufficiently explored. However, when the number of tasks is high, we may not be able to derive reasonable ground truth Pareto fronts using direct brute-force search. Nonetheless, we can still demonstrate the efficiency of our method by comparing the winning ratio of LocMAP and direct brute-force search.

2 BACKGROUND

2.1 MODEL MERGING

Model merging aims to combine two or more trained models into a single model to leverage the strengths of each and improve overall performance. A recent work by Ilharco et al. (2022) introduced *task arithmetic* as a simple and effective way to perform model merging. The task vector for task n is defined as $\mathbf{v}_n = \theta_{ft}^n - \theta_{pre}$, which is the element-wise difference between the pre-trained weights and the fine-tuned weights for task n . To perform model merging with task vectors, we can compute the merged model as $\theta_m = \theta_{pre} + \sum_{n=1}^N c_n \mathbf{v}_n$, where c_n are the scaling coefficients that have been shown to be essential to the performance of the merged model Yadav et al. (2024); Yang et al. (2023).

Denoting the metric of task n as M_n , most of the existing approaches for model merging aim to improve an equal weight average metric $\frac{1}{N} \sum_{n=1}^N M_n$. This target implies that user of the algorithm has no preferences between tasks. However, in real-world applications, users might have biased preferences for the importance of tasks, necessitating trade-offs. In such cases, the goal of model merging is no longer the simple average metric. Instead, we need to answer a broader question:

Given any preferences over the set of tasks, what is the best way to merge the models?

2.2 PARETO FRONTS

Definition 1 (Pareto dominance). *Let X be a set representing the solution space, where each element $x \in X$ is a possible solution to the multi-objective optimization problem. Let there be n objectives, and define an evaluation loss function $f_i : X \rightarrow \mathbb{R}$, where $i \in \{1, 2, \dots, n\}$.*

Given two solutions $x, y \in X$, we define that x Pareto dominates y , denoted by $x \succ_P y$, if and only if:

$$\forall i \in \{1, 2, \dots, n\}, f_i(x) \leq f_i(y) \text{ and } \exists j \in \{1, 2, \dots, n\}, f_j(x) < f_j(y)$$

Definition 2 (Pareto optimal solutions). *The Pareto front is the set of solutions in the solution space X that are not Pareto dominated by any other solutions in X . The Pareto front is given by:*

$$PF = \{x \in X \mid \nexists y \in X \text{ s.t. } y \succ_P x\} \quad (1)$$

Pareto optimal solutions have been studied in multi-task (multi-objective) learning (MTL) Sener & Koltun (2018); Lin et al. (2019). However, in most of the studies, approximating the Pareto front is computationally expensive and data inefficient. We introduce our method, LocMAP, a computationally efficient method to find the Pareto front for model merging.

3 METHODS

In this section, we discuss the proposed LocMAP method in detail. To enhance readability, we present a table of notations in Table 5.

3.1 QUADRATIC APPROXIMATION OF EVALUATION METRIC

Given the task vectors $\{\mathbf{v}_n\}_{\{n=1,\dots,N\}}$ and the initialization $\boldsymbol{\theta}_{\text{pre}} \in \mathbb{R}^d$, we denote the merged model parameters as $\boldsymbol{\theta}_m(\mathbf{c}) = \boldsymbol{\theta}_{\text{pre}} + \mathbf{V}\mathbf{c} = \boldsymbol{\theta}_{\text{pre}} + \sum_{n=1}^N c_n \mathbf{v}_n$, where $\mathbf{V} = \text{concat}(\mathbf{v}_1, \dots, \mathbf{v}_N) \in \mathbb{R}^{d \times N}$ is the task matrix and $\mathbf{c} = [c_1, \dots, c_N]^\top \in \mathbb{R}^N$ is the vector of scaling coefficients for the task vectors.

Let $M_n(\mathbf{c}) = M_n(\boldsymbol{\theta}_m(\mathbf{c}))$ denote the evaluation metric for task n of the merged model. We aim to optimize the evaluation metric for each task via the multi-objective optimization (MOOP)¹:

$$\min_{c_1, \dots, c_N} M_1(\mathbf{c}), \dots, M_N(\mathbf{c}) \quad (2)$$

This problem has N variables and N objectives, and we seek the Pareto optimal solutions.

Motivated by the observation that the finetuned models tend to have parameters close to the pretrained model (as shown in Table 1), we put forward the following assumption.

Assumption 1. *The task vectors \mathbf{v}_n have small norms relative to the pretrained model parameters $\boldsymbol{\theta}_{\text{pre}}$, i.e., $|\mathbf{v}_n| \ll |\boldsymbol{\theta}_{\text{pre}}|$ for $n = 1, \dots, N$. Additionally, the evaluation metrics $M_n(\boldsymbol{\theta})$ are sufficiently smooth around $\boldsymbol{\theta}_{\text{pre}}$, such that higher-order terms in their Taylor expansions are negligible within the region defined by the task vectors.*

Denote p as the number of parameters in the pre-trained model and also the number of parameters in each task vector. N is the number of tasks.

To derive our algorithm, LocMAP, we utilize the second-order Taylor expansion to approximate M_n :

$$\begin{aligned} M_n(\mathbf{c}) &\equiv M_n(\boldsymbol{\theta}_m(\mathbf{c})) = M_n(\boldsymbol{\theta}_{\text{pre}}) + \nabla M_n(\boldsymbol{\theta}_{\text{pre}})^\top (\boldsymbol{\theta}_m(\mathbf{c}) - \boldsymbol{\theta}_{\text{pre}}) \\ &\quad + \frac{1}{2} (\boldsymbol{\theta}_m(\mathbf{c}) - \boldsymbol{\theta}_{\text{pre}})^\top \mathbf{H}_n(\boldsymbol{\theta}_{\text{pre}}) (\boldsymbol{\theta}_m(\mathbf{c}) - \boldsymbol{\theta}_{\text{pre}}) + R_n(\boldsymbol{\theta}_m(\mathbf{c}) - \boldsymbol{\theta}_{\text{pre}}) \\ &= \underbrace{M_n(\boldsymbol{\theta}_{\text{pre}})}_{\in \mathbb{R}} + \underbrace{\nabla M_n(\boldsymbol{\theta}_{\text{pre}})^\top}_{\in \mathbb{R}^{1 \times p}} \underbrace{\mathbf{V}}_{\in \mathbb{R}^{p \times N}} \underbrace{\mathbf{c}}_{\in \mathbb{R}^{N \times 1}} + \frac{1}{2} \underbrace{(\mathbf{V}\mathbf{c})^\top}_{\in \mathbb{R}^{1 \times p}} \underbrace{\mathbf{H}_n(\boldsymbol{\theta}_{\text{pre}})}_{\in \mathbb{R}^{p \times p}} \underbrace{\mathbf{V}\mathbf{c}}_{\in \mathbb{R}^{p \times 1}} + \underbrace{R_n}_{\in \mathbb{R}} \end{aligned}$$

where $\mathbf{H}_n(\boldsymbol{\theta}_{\text{pre}}) = \nabla^2 M_n(\boldsymbol{\theta}_{\text{pre}}) \in \mathbb{R}^{d \times d}$ is the Hessian matrix and $R_n(\boldsymbol{\theta}_m(\mathbf{c}) - \boldsymbol{\theta}_{\text{pre}}) = R_n(\mathbf{V}\mathbf{c})$ is the third-order remainder, which in Assumption 1, is negligible when $\|\mathbf{V}\mathbf{c}\|^3 = \|\boldsymbol{\theta}_m(\mathbf{c}) - \boldsymbol{\theta}_{\text{pre}}\|^3$ is small. Note that the second-order Taylor expansion is widely used McCandlish et al. (2018); Bu et al. (2024); Kaplan et al. (2020); Hoffmann et al. (2022) and provides a close approximation (see Figure 2 (a) and (b) and more discussion in Appendix 5).

Table 1: We compute the L_1 norm of the weight matrices of the pretrained models and the task vectors for each of the 8 tasks using the ViT-B/32 model, and compute the ratio.

Metric	SUN397	Cars	DTD	SVHN	RESISC45	MNIST	GTSRB	EuroSAT
$\ \boldsymbol{\theta}_{\text{pre}}\ _1$	1,270,487	1,270,487	1,270,487	1,270,487	1,270,487	1,270,487	1,270,487	1,270,487
$\ \mathbf{v}_n\ _1$	21,055	20,127	13,621	19,349	18,409	17,578	16,712	15,941
$\ \mathbf{v}_n\ _1 / \ \boldsymbol{\theta}_{\text{pre}}\ _1 (\%)$	1.66%	1.58%	1.07%	1.52%	1.45%	1.38%	1.32%	1.25%

¹The evaluation metric M can be differentiable (e.g., mean square loss or cross-entropy/perplexity) or not necessarily (e.g., classification accuracy, F1 score, BLEU, or Rouge)

To validate the approximation, we calculate the L_1 norm of the parameters for the 8 task vectors and their ratios relative to the L_1 norm of the pretrained model. As shown in Table 1, the ratio between the L_1 norm of the task vectors and the L_1 norm of the weight matrices of the pretrained model is approximately 1% to 2% for each of the 8 tasks.

We further examine the density plot of the absolute values of the weight matrices of the 8 task vectors (Figure 3). We find that the maximum magnitude of the task vectors is 0.00859, while the mean is 1.57336×10^{-4} . These findings motivate and validate our key assumption 1 of using a second-order Taylor expansion to approximate the evaluation metrics.

Leveraging this quadratic approximation, we can define surrogate models for each task N ,

$$\tilde{M}_n(\mathbf{c}; \mathbf{A}_n, \mathbf{b}_n, e_n) \equiv \frac{1}{2} \mathbf{c}^\top \mathbf{A}_n \mathbf{c} + \mathbf{b}_n^\top \mathbf{c} + e_n \quad (3)$$

and optimize the proxy problem of Equation (2) via

$$\min_{c_1, \dots, c_N} \tilde{M}_1(\mathbf{c}), \dots, \tilde{M}_N(\mathbf{c}) \quad (4)$$

where $\mathbf{A}_n \in \mathbb{R}^{N \times N}$ is a parameterized matrix aiming to approximate $\mathbf{V}^\top \mathbf{H}_n(\boldsymbol{\theta}_{\text{pre}}) \mathbf{V}$; $\mathbf{b}_n \in \mathbb{R}^N$ is a parameterized vector targeting to $\mathbf{V}^\top \nabla M_n(\boldsymbol{\theta}_{\text{pre}})$; e_n is a parameter scalar which estimates $M_n(\boldsymbol{\theta}_{\text{pre}}) + R_n$.

Importantly, Equation (4) is parameterized in contrast to Equation (2), with a total of $\frac{(N+1)(N+2)}{2}$ surrogate model parameters in $(e_n, \mathbf{b}_n, \mathbf{A}_n)$, i.e., 1 coefficient for e_n , N coefficients in \mathbf{b}_n and $N(N+1)/2$ coefficients in \mathbf{A}_n due to its symmetry ($1 + N + \frac{N(N+1)}{2} = \frac{(N+1)(N+2)}{2}$). We do not calculate the gradient or Hessian to obtain the parameters $\mathbf{A}_n, \mathbf{b}_n, e_n$. Instead, we estimate them by minimizing the MSE between M_n and \tilde{M}_n , $n = 1, \dots, N$:

$$\mathbf{A}_n^*, \mathbf{b}_n^*, e_n^* = \arg \min_{\mathbf{A}_n, \mathbf{b}_n, e_n} \sum_{\mathbf{c} \in \Omega} |M_n(\boldsymbol{\theta}_{\text{merge}}(\mathbf{c})) - \tilde{M}_n(\mathbf{c}; \mathbf{A}_n, \mathbf{b}_n, e_n)|^2 \quad (5)$$

where $\Omega = \{\mathbf{c}^{(1)}, \dots, \mathbf{c}^{(K)}\}$ is the set of \mathbf{c} and $M_n(\boldsymbol{\theta}_{\text{merge}}(\mathbf{c}))$ is the corresponding evaluation metric. Below we discuss 3 extensive cases of this problem.

Case 1: If the evaluation metric spans the whole real-number axis \mathbb{R} , we use the vanilla form of the surrogate model in Equation (3). As shown in Corollary 1, we have a closed-form solution for Equation (5)

Corollary 1 (Closed-form Solution for Surrogate Model Parameters). *Under Assumption 1, for each task $n = 1, \dots, N$, the optimization problem 5 is equivalent to solving a linear regression where the predictors include all quadratic, interaction, linear, and constant terms of \mathbf{c} . The closed-form solution for the parameters is given by*

$$\begin{pmatrix} \text{vec}(\mathbf{A}_n^*) \\ \mathbf{b}_n^* \\ e_n^* \end{pmatrix} = (\mathbf{C}_n^\top \mathbf{C}_n)^{-1} \mathbf{C}_n^\top \mathbf{y}_n$$

where $\mathbf{C}_n(\mathbf{c}) = (c_1^2, c_2^2, \dots, c_N^2, c_1 c_2, c_1 c_3, \dots, c_{N-1} c_N, c_1, c_2, \dots, c_N, 1)$, and \mathbf{y}_n is the vector of observed metrics $M_n(\boldsymbol{\theta}_m(\mathbf{c}))$ for all $\mathbf{c} \in \Omega$. Please refer to Corollary 3 for a more detailed corollary.

Case 2: When the evaluation metric is restricted to a specific range $[l, u]$, e.g. accuracy is restricted to $[0, 1]$, we can warp the quadratic part using a sigmoid function, i.e.

$$\tilde{M}_n(\mathbf{c}; \mathbf{A}_n, \mathbf{b}_n, e_n) \equiv (u - l) \sigma(e_n + \mathbf{b}_n^\top \mathbf{c} + \frac{1}{2} \mathbf{c}^\top \mathbf{A}_n \mathbf{c}) + l.$$

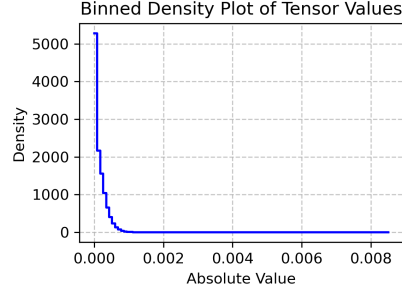


Figure 3: Density plot of the absolute values of the weight matrices of the 8 task vectors.

Case 3: Similarly, if the evaluation metric is restricted to $[l, +\infty)$, a softplus function as a wrapper would be beneficial:

$$\tilde{M}_n(\mathbf{c}; \mathbf{A}_n, \mathbf{b}_n, e_n) \equiv \text{softplus}(e_n + \mathbf{b}_n^\top \mathbf{c} + \frac{1}{2} \mathbf{c}^\top \mathbf{A}_n \mathbf{c}) + l,$$

where $\text{softplus}(x) = \ln(1 + e^x)$.

In Cases 2 and 3, please note that u and l mentioned here are not learnable parameters. They are specific to the feasible area of the metric. Since the non-linear functions are introduced in the definition of \tilde{M}_n , there are no closed-form solutions. We use gradient descent to solve the optimization problem 5. This approach remains fast and computationally inexpensive, as the number of parameters in the surrogate model is $\frac{(N+1)(N+2)}{2}$. We emphasize that performing gradient descent on the surrogate model remains computationally efficient. Compared to training full-scale deep learning models, it requires significantly fewer computations, making it both faster and more resource-efficient. In the case of merging 8 models, the number of parameters is 45 which is significantly less than the millions of parameters typically found in deep learning models.

3.2 MODEL MERGING WITH AMORTIZED PARETO FRONTS

In this section, we introduce our generalized algorithm for estimating the amortized Pareto fronts. As mentioned in Section 3.1, we approximate the evaluation metric $M_n(\cdot)$ by a surrogate quadratic model $\tilde{M}_n(\cdot)$. We then utilize $\tilde{M}_n(\cdot)$ to compute the amortized Pareto fronts. Please see the detailed experiments in Section 4 and the algorithm details in Algorithm 1. Different from other Pareto multi-task learning algorithms, our algorithm does not require calculating the gradients or performing gradient descent on the deep learning model parameters.

Algorithm 1 LocMAP

Input: Pretrained model θ_{pre} , fine-tuned models $\{\theta_{ft}^n\}_{n=1}^N$.

Compute task vectors $\{\mathbf{v}_n = \theta_{ft}^n - \theta_{pre} \mid n \in 1, \dots, N\}$.

Sample K vectors of $\mathbf{c} \in \mathbb{R}^N$. Denote the set as Ω .

for $n \in [N]$ **do**

for $\mathbf{c} = [c_1, \dots, c_N] \in \Omega$ **do**

 Compute $\theta(\mathbf{c}) = \theta_{pre} + c_1 \mathbf{v}_1 + \dots + c_N \mathbf{v}_N$.

 Derive the evaluation metric $M_n(\theta(\mathbf{c}))$.

end

 Fit the quadratic approximation surrogate model \tilde{M}_n by learning \mathbf{A}_n^* , \mathbf{b}_n^* , e_n^* in Equation (5).

end

Apply MOOP algorithm (e.g. NSGA-III) to $\{\tilde{M}_n\}$ and get the Pareto front

3.3 FURTHER METHODS TO BRING DOWN THE COMPUTATION COST WHEN THE NUMBER OF TASKS IS HIGH

In addition to LocMAP, we also introduce LocMAP variants, nested merging LocMAP (NMLocMAP) and Bayesian LocMAP (BLocMAP). NMLocMAP and BLocMAP are LocMAP variants designed to further reduce the computation of LocMAP.

For a small number of tasks ($N \leq 3$), we use Bayesian adaptive sampling, inspired by Bayesian optimization. Unlike the Plain LocMAP (Algorithm 1), which samples a single set of scaling weights \mathbf{c} and evaluates metrics $M_n(\theta(\mathbf{c}))$, Bayesian adaptive sampling iteratively samples \mathbf{c} across multiple rounds, with each round informed by prior evaluations.

The process starts with uniform sampling of scaling coefficients $\{(c_1, \dots, c_N)\}$, from $[0, 1]^N$, evaluating the merged models $\theta_m(\mathbf{c}_i)$ for tasks 1 to N , and calculating the L_2 loss. We compute a posterior distribution based on an acquisition function, like the upper confidence bound, for each bin.

We iteratively update surrogate models for each task, and after meeting the stopping criterion, generate $(\mathbf{c}, \{\tilde{M}_n(\theta_m(\mathbf{c}))\}_{n=1}^N)$ samples. A MOOP algorithm (e.g., NSGA-III) is then applied to compute the Pareto front from \tilde{M}_n .

As illustrated in Figure 4 (a), BLocMAP uses Bayesian optimization to determine the distribution of scaling coefficients for task vectors when approximating the surrogate model in LocMAP. For more details and experiments, please refer to Appendix E.3.

When the number of tasks N is high and computational resources are also limited, NMLocMAP reduces the number of evaluations from $O(TN2^N)$ to $O(N \log N)$. For example, tasks 1 to 8 are Cars, GTSRB, DTD, SUN397, Resisc45, MNIST, EuroSAT, and SVHN.

With the nested merging, for the first round, we merge $(\theta_{ft}^1, \theta_{ft}^2)$ into $\theta_{merge}^{1,2}$. Similarly, we merge $(\theta_{ft}^3, \theta_{ft}^4)$ into $\theta_{merge}^{3,4}$, and $(\theta_{ft}^5, \theta_{ft}^6)$ into $\theta_{merge}^{5,6}$. Next, we merge $(\theta_{merge}^{1,2}, \theta_{merge}^{3,4})$ into $\theta_{merge}^{1,2,3,4}$, and finally into $\theta_{merge}^{1,2,3,4,5,6,7,8}$.

It achieves a 250x speedup when the number of tasks is 8, while also outperforming direct search methods. However, it can no longer output the entire Pareto front for all tasks, and the practitioners need to be able to quantify their preferences during the merging since it merges models in pairs in nested fashion, as shown in Figure 4 (b). For more details and experiments, please refer to Appendix E.2.

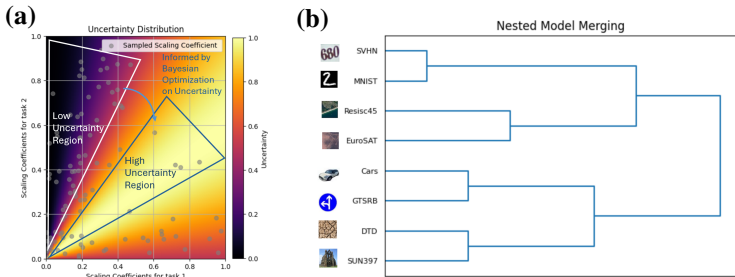


Figure 4: **Subfigure (a)** Utilize Bayesian optimization to guide the sampling of scaling coefficients according to uncertainty distribution; **Subfigure (b)** An example of nested model merging for $N = 8$ models.

4 EXPERIMENTS

Datasets and models We study multi-task model merging on eight normal zero-shot image classification datasets following Ilharco et al. (2022): SUN397 Xiao et al. (2016), Cars Krause et al. (2013), GTSRB Stallkamp et al. (2011), MNIST LeCun (1998), EuroSAT Helber et al. (2019), SHVN Netzer et al. (2011), DTD Cimpoi et al. (2014), RESISC45 Cheng et al. (2017). We use the ViT-B/32 architecture in CLIP Radford et al. (2021) as the pre-trained model for the experiments on vision tasks in the main text. We show the results of these experiments in the main pages.

The rest of the experiments are presented in the Appendix due to the page limits. The results of the datasets and tasks we experimented on are as follows: a zero-shot medical chest X-ray image classification task to show our model merging scheme also works in a real-world application in the medical domain Wang et al. (2017) (Appendix D.3); 4 fine-tuned Llama3 models in different languages: French, Arabic, Chinese, and Japanese (Appendix D.4)²; 3 vision tasks on the ResNet18 He et al. (2016) architecture: CIFAR-10 Krizhevsky et al. (2009), Flowers-102 Nilsback & Zisserman (2008), and GTSRB Stallkamp et al. (2011) to show our model merging scheme also works on other model architectures (Appendix D.5).

4.1 BASELINE AND METRICS

Pareto front-finding baselines One of our baseline methods for obtaining Pareto fronts is the brute-force direct search, which can be regarded as the gold standard when the number of tasks is low ($N < 4$). This is because we can sample enough grid points of \mathbf{c} and query the corresponding

²All the fine-tuned language Llama3 models can be found on Hugging Face. The IDs of the models are: French: jpacifico/French-Alpaca-Llama3-8B-Instruct-v1.0; Arabic: MohamedRashad/Arabic-Orpo-Llama-3-8B-Instruct; Chinese: shenzhi-wang/Llama3-8B-Chinese-Chat; Japanese: haqishen/Llama-3-8B-Japanese-Instruct.

evaluation metrics $\{M_n(\theta(\mathbf{c}))\}_{n=1}^N$. We can then directly use the resulting evaluation metrics to find the Pareto front by direct comparisons of each task’s performance of the merged model by $c_i \in \mathbf{c}$.

Another baseline method for finding Pareto fronts is the Multi-Objective Evolutionary Algorithm based on Decomposition (MOEA/D) Zhang & Li (2007). Key hyperparameters in MOEA/D include the population size and the number of generations, which significantly influence its performance by affecting the quality and diversity of the resulting Pareto front as well as the computational cost.

It is important to note that when the number of tasks grows, the required number of $(\mathbf{c}, \{M_n(\theta(\mathbf{c}))\}_{n=1}^N)$ pairs grows exponentially for the brute force method, as well as for the MOEA/D method, which is much larger than the points we can evaluate given the computational constraint. Thus, when the number of tasks is high ($N \geq 4$), the results from the brute-force direct search can no longer be considered ground truth. In Appendix E.2.2, we show an illustration of why the curse of dimensionality occurs when the number of tasks increases.

Single merged model baselines In addition to the brute-force method and MOEA/D, we compare with other model merging methods including SLERP Shoemake (1985), TIES-merging Yadav et al. (2024), Task Arithmetic with a single scalar Ilharco et al. (2022), Task Arithmetic with preferences as scalars Ilharco et al. (2022), DARE combined with Task Arithmetic Yu et al. (2023); Ilharco et al. (2022), and DARE combined with TIES-merging Yu et al. (2023); Yadav et al. (2024).

Win rate We used the win rate to measure how often the Pareto front found by LocMAP outperforms the Pareto front found by the baseline in terms of multiple objectives. Let PF_{LocMAP} and $PF_{baseline}$ represent the set of solutions in the Pareto fronts obtained from the LocMAP and the baseline methods, respectively. Each solution in these sets is a vector in \mathbb{R}^N , where N is the number of objectives or tasks. We sampled $K = 100$ points from the decision space of each of the two Pareto fronts, denoted as \mathbf{c}_k^{LocMAP} and $\mathbf{c}_k^{baseline}$, $k = 1, \dots, K$. Then, we compared $M_n(\theta(\mathbf{c}_k^{LocMAP}))$ and $M_n(\theta(\mathbf{c}_k^{baseline}))$ pairwise for $k = 1, \dots, K$ and $n = 1, \dots, N$, resulting in K^2N comparisons. The ratio of instances where $M_n(\theta(\mathbf{c}_k^{LocMAP})) > M_n(\theta(\mathbf{c}_k^{baseline}))$ is computed as the win rate of PF_{LocMAP} :

$$\text{Win Rate} = \frac{1}{K^2N} \sum_{i=1}^K \sum_{j=1}^K \sum_{n=1}^N \mathbb{I} [M_n(\theta(\mathbf{c}_i^{LocMAP})) > M_n(\theta(\mathbf{c}_j^{baseline}))]$$

where $K = 100$, $\mathbf{c}_i^{LocMAP} \in \text{Decision Space of } PF_{LocMAP}$, $i = 1, \dots, K$, $\mathbf{c}_j^{baseline} \in \text{Decision Space of } PF_{baseline}$, $j = 1, \dots, K$, $\mathbb{I}[\cdot]$ is the indicator function.

4.2 WIN RATE OF LOCMAP OVER THE DIRECT SEARCH METHOD

Table 2 shows the results for the win rate of LocMAP over the brute force direct search method **when the number of tasks is small** ($N < 4$). In such cases, the Pareto front can be regarded as the ground truth Pareto front, and we can only query 30 and 50 scaling coefficients to achieve similar performance with the ground truth Pareto front.

Table 3 shows the results for the win rate of LocMAP over the brute force direct search method **when the number of tasks is high** ($N \geq 4$). The Pareto front generated by the brute force method can no longer be considered ground truth due to the limited number of points per dimension that is covered. In this setting, LocMAP performs much better than the brute-force (not ground truth) Pareto solutions.

Table 2: Win rate of the amortized PF over the brute-force direct search PF, where the latter can be regarded as the ground truth when $N < 4$. # \mathbf{c} is the number of scaling coefficient vectors each algorithm evaluated to find the Pareto front. # \mathbf{c} per dim = (# \mathbf{c} direct search) $^{1/N}$ measures the sparsity of points the direct search method uses, as illustrated in Figure 11.

N	# \mathbf{c} (direct search)	# \mathbf{c} per dim	# \mathbf{c} (LocMAP)	Win rate (LocMAP)	R^2 (LocMAP)
2	200	14.14	30	49.81% (± 0.30)	0.953 (± 0.018)
3	300	6.69	50	46.90% (± 0.71)	0.980 (± 0.003)

4.3 COMPARING WITH OTHER SINGLE MERGED MODEL BASELINE METHODS

We compared the performance of LocMAP with TIES-merging Yadav et al. (2023), TIES-merging with DARE Yu et al. (2023), Task Arithmetic with DARE, Task Arithmetic with normalized preference

Table 3: Win rate of the amortized PF over the brute-force direct search PF, where the latter can **no longer** be regarded as the ground truth when $N \geq 4$. # of c is the number of scaling coefficient vectors each algorithm evaluated to find the Pareto front. # c per dim = (# c direct search) $^{1/N}$ measures the sparsity of points the direct search method uses, as illustrated in Figure 11.

N	# c (direct search)	# c per dim	# c (LocMAP)	Win rate (LocMAP)	R^2 (LocMAP)
4	300	4.16	60	50.67% (± 2.44)	0.984 (± 0.004)
5	500	3.47	85	53.00% (± 1.88)	0.941 (± 0.019)
6	500	2.82	100	60.71% (± 1.34)	0.941 (± 0.030)
7	1000	2.68	140	63.42% (± 1.91)	0.891 (± 0.024)
8	1000	2.37	250	65.58% (± 0.94)	0.868 (± 0.028)

as scaling coefficients Ilharco et al. (2023), Ada-mgering++ Yang et al. (2024), DELLA-merging Deep et al. (2024) and SLERP Shoemake (1985). For dimension 2, we can directly visualize the results, as shown in Figure 5. As we can observe, the solutions found by MOEA/D exhibited clustering and a lack of adequate spread across the Pareto front. In addition, the computational cost of MOEA/D was significantly higher than that of LocMAP. For example, with a population size of 50 and 20 generations (which produced the best results for MOEA/D in terms of diversity as shown in Figure 5), the total number of evaluations amounted to 2500 for two tasks. In comparison, LocMAP achieved its results with only 60 total evaluations—a reduction of over 95%. This highlights the computational efficiency of LocMAP in obtaining a diverse and high-quality Pareto front.

LocMAP offers a well-distributed set of Pareto optimal solutions We can see that none of the baseline methods can directly dominate all Pareto solutions found by LocMAP, and most of them lie either within or on the Pareto front found by LocMAP. In addition, we sampled 10 points from the predicted Pareto front by LocMAP and evaluated them (LocMAP Pareto solutions, real) to confirm that they indeed lie close to the predicted Pareto front. This evidence further confirms the usefulness of LocMAP as a general strategy for finding a set of diverse and well-distributed Pareto solutions that none of the existing model merging methods can substitute.

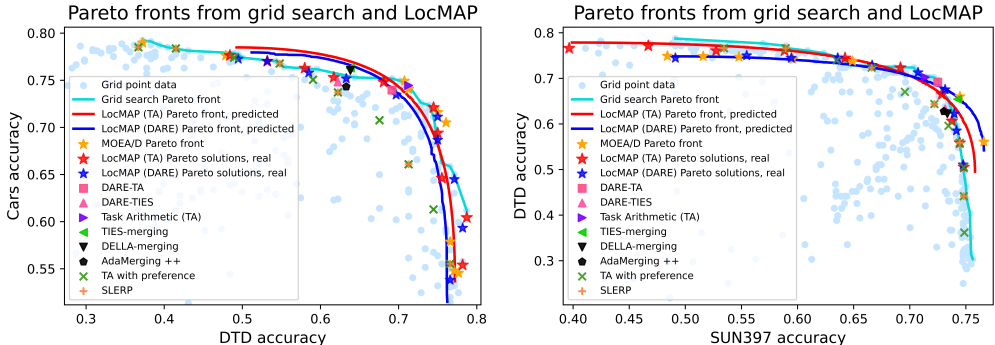


Figure 5: The Pareto fronts obtained using LocMAP with Task Arithmetic, LocMAP with Task Arithmetic and DARE. We sampled 10 Pareto solutions from the predicted front by LocMAP and evaluated them to obtain the real values. We plotted the results obtained using TIES-merging, Task Arithmetic (TA) with a single scalar for all tasks, Task Arithmetic with preferences as scalars, TA combined with DARE (DARE-TA), TIES-merging combined with DARE (DARE-TIES), and SLERP.

LocMAP is an out-of-the-box plugin for other task-vector based model merging methods As shown in Figure 5, LocMAP is a plug-in that can be directly combined with other model merging methods where the users can control their preferences over each task using some scaling coefficients. For example, LocMAP can be combined with DARE, Task Arithmetic, etc.

For dimensions higher than 2, we use preference-weighted evaluation sum to compare the Pareto front found by LocMAP with other baseline methods. We sample 20 preference vectors and normalize them. Then, we pick the solution by LocMAP that maximizes the preference-weighted sum of accuracies and compare it with those of the baseline methods. The results are shown in Table 4. We can observe that even in higher dimensions, when the user has certain preferences, LocMAP is still useful and can better accommodate user preferences. Please note that when using LocMAP, we do

not require the user to pre-specify their preference vector. In fact, the users can get the entire Pareto front to better understand the trade-offs. This preference vector based metric is only for evaluation.

Table 4: We compared LocMAP with a set of baseline methods by sampling a set of 20 normalized preference vectors and computing the preference-weighted sum of accuracies. \uparrow indicates higher is better. The number after \pm is the standard deviation. Please refer to Table 2 and Table 3 for the number of scaling coefficient vectors used for different numbers of tasks.

# tasks	Preference weighted sum of accuracies (\uparrow)							
	2	3	4	5	6	7	8	
Single task models	75.84 \pm 1.76	77.03 \pm 1.84	82.43 \pm 4.40	87.69 \pm 4.50	88.52 \pm 4.02	89.26 \pm 3.58	90.62 \pm 2.52	
MTL	73.63 \pm 0.30	75.13 \pm 1.00	80.10 \pm 2.79	84.93 \pm 3.58	86.78 \pm 2.94	87.40 \pm 2.56	89.11 \pm 2.36	
Model soups (Wortsman et al. (2022a))	67.79 \pm 1.46	64.25 \pm 2.15	66.04 \pm 3.22	67.01 \pm 3.42	63.11 \pm 1.99	63.35 \pm 2.17	64.36 \pm 2.77	
TIES-merging (Yadav et al. (2024))	69.30 \pm 0.33	67.60 \pm 0.58	71.79 \pm 2.93	76.49 \pm 3.10	73.74 \pm 2.96	72.54 \pm 2.87	72.24 \pm 1.91	
DARE-TIES	67.62 \pm 1.65	66.49 \pm 2.34	71.39 \pm 4.45	74.55 \pm 4.55	73.34 \pm 4.10	71.43 \pm 3.84	71.89 \pm 2.86	
Task Arithmetic (Ilharco et al. (2022))	70.73\pm1.84	61.15 \pm 2.33	52.69 \pm 4.23	61.58 \pm 4.62	51.37 \pm 3.84	39.79 \pm 3.97	60.77 \pm 2.84	
TA with preference as weights	69.22 \pm 1.4	66.88 \pm 2.37	68.73 \pm 5.48	71.92 \pm 5.5	68.13 \pm 4.69	68.14 \pm 4.2	68.17 \pm 2.89	
DARE-TA	70.61 \pm 0.22	64.18 \pm 1.24	58.04 \pm 8.19	65.39 \pm 7.03	56.76 \pm 7.01	46.75 \pm 5.73	64.51 \pm 3.81	
Ada-Merging++ (Yang et al. (2024))	67.27 \pm 1.92	67.13 \pm 1.92	71.19 \pm 4.43	76.84 \pm 4.71	74.13 \pm 4.07	72.58 \pm 4.16	72.55 \pm 2.83	
DELLA-Merging (Deep et al. (2024))	67.10 \pm 2.08	65.92 \pm 2.48	70.71 \pm 4.31	74.43 \pm 4.32	72.64 \pm 3.77	71.16 \pm 3.95	71.49 \pm 2.83	
MOEA/D	70.22 \pm 1.46	67.94 \pm 1.79	70.85 \pm 4.58	72.03 \pm 4.03	67.88 \pm 3.09	69.06 \pm 2.97	68.59 \pm 2.89	
LocMAP	70.7 \pm 1.76	69.05\pm1.84	72.84\pm4.4	77.31\pm4.5	74.26\pm4.02	73.40\pm3.58	72.96\pm2.52	

5 RELATED WORK

Due to space constraints, for a more comprehensive discussion, please refer to Appendix B.

Multi-objective optimization Multi-objective optimization (MOOP) identifies diverse Pareto solutions with different trade-offs. The multi-task problem has been approached from a MOOP perspective Sener & Koltun (2018); Lin et al. (2019), utilizing algorithms like MGDA, IMTL, GradNorm, RLW, and scalarization. While these methods iteratively optimize \mathbb{R}^d model parameters with significant computational cost, our approach performs post-training MOOP over \mathbb{R}^N scaling coefficients, reducing computational burden. For $N \geq 3$ objectives, MOOP becomes many-objective optimization, challenging traditional algorithms (e.g. NSGA-II and SPEA2). Advanced methods such as ϵ -MOEA Deb et al. (2003), MSOPS Hughes (2005), SMS-EMOA Beume et al. (2007), and NSGA-III Deb & Jain (2013), or the KKT approach Augusto et al. (2014) are required. Selection factors include solution quality and computational efficiency, noting that some methods like hypervolume indicators Auger et al. (2009) have super-polynomial time complexity with objective count.

Task arithmetic Task arithmetic, a model merging method gaining attention, uses weighted averages of models for multi-task performance. Various approaches exist for selecting scaling coefficients Ilharco et al. (2022); Yadav et al. (2024); Yang et al. (2023): Ilharco et al. (2022) uses equal scaling, which is suboptimal and limited; Yang et al. (2023) optimizes weights using Shannon entropy but requires unlabeled test data, conflicting with data privacy goals in model merging Matena & Raffel (2022) and only applies to classification tasks. Wortsman et al. (2022b)’s ‘WiSE-FIT’ averages pre-trained and fine-tuned parameters for trade-offs. Task Arithmetic Ilharco et al. (2022) adds weighted differences between fine-tuned and pre-trained models. Ortiz-Jiménez et al. (2023) enhanced weight disentanglement through tangent space fine-tuning. Beyond task arithmetic, Ainsworth et al. (2023) merge models via weight matrix permutations, even without shared pretraining. Jin et al. (2023) introduced dataless knowledge fusion. Daheim et al. (2024) proposed uncertainty-based gradient matching for improved merging performance and robustness.

6 CONCLUSION AND LIMITATIONS

We introduced LocMAP, a novel low-compute approach to efficiently merge models while accounting for trade-offs between multiple tasks. By leveraging a quadratic approximation of the evaluation metrics, LocMAP successfully identifies amortized Pareto fronts without the need for gradient descent for deep neural networks. The algorithm’s efficiency is further enhanced through Bayesian adaptive sampling and nested merging, enabling it to scale to problems with a higher number of tasks. Moreover, LocMAP is an out-of-the-box plug-in for other task-vector-based model merging methods.

However, we would like to point out some limitations of our method. We do not have a detector algorithm to detect if two tasks have proper trade-offs. Approximating a Pareto "front" with only a single Pareto solution can lead to degenerate solutions. In this case, practitioners should be informed.

REFERENCES

- 540
541
542 Samuel K. Ainsworth, Jonathan Hayase, and Siddhartha S. Srinivasa. Git re-basin: Merging mod-
543 els modulo permutation symmetries. In *The Eleventh International Conference on Learning*
544 *Representations, ICLR 2023, Kigali, Rwanda, May 1-5, 2023*. OpenReview.net, 2023. URL
545 <https://openreview.net/pdf?id=CQsmMYm1P5T>.
- 546 Zeyuan Allen-Zhu, Yuanzhi Li, and Zhao Song. A convergence theory for deep learning via over-
547 parameterization. In *International conference on machine learning*, pp. 242–252. PMLR, 2019.
- 548 Anne Auger, Johannes Bader, Dimo Brockhoff, and Eckart Zitzler. Theory of the hypervolume
549 indicator: optimal μ -distributions and the choice of the reference point. In *Proceedings of the tenth*
550 *ACM SIGEVO workshop on Foundations of genetic algorithms*, pp. 87–102, 2009.
- 551
552 Oscar Brito Augusto, Fouad Bennis, Stephane Caro, et al. Multiobjective optimization involving
553 quadratic functions. *Journal of optimization*, 2014, 2014.
- 554
555 Nicola Beume, Boris Naujoks, and Michael Emmerich. Sms-emoa: Multiobjective selection based
556 on dominated hypervolume. *European Journal of Operational Research*, 181(3):1653–1669, 2007.
- 557 Tom Brown, Benjamin Mann, Nick Ryder, Melanie Subbiah, Jared D Kaplan, Prafulla Dhariwal,
558 Arvind Neelakantan, Pranav Shyam, Girish Sastry, Amanda Askell, et al. Language models are
559 few-shot learners. *Advances in neural information processing systems*, 33:1877–1901, 2020.
- 560
561 Zhiqi Bu, Xinwei Zhang, Mingyi Hong, Sheng Zha, and George Karypis. Pre-training differentially
562 private models with limited public data. *arXiv preprint arXiv:2402.18752*, 2024.
- 563 Sébastien Bubeck et al. Convex optimization: Algorithms and complexity. *Foundations and Trends®*
564 *in Machine Learning*, 8(3-4):231–357, 2015.
- 565
566 Gong Cheng, Junwei Han, and Xiaoqiang Lu. Remote sensing image scene classification: Benchmark
567 and state of the art. *Proceedings of the IEEE*, 105(10):1865–1883, 2017.
- 568
569 Lenaïc Chizat, Edouard Oyallon, and Francis Bach. On lazy training in differentiable programming.
570 *Advances in neural information processing systems*, 32, 2019.
- 571
572 Mircea Cimpoi, Subhansu Maji, Iasonas Kokkinos, Sammy Mohamed, and Andrea Vedaldi. Describ-
573 ing textures in the wild. In *Proceedings of the IEEE conference on computer vision and pattern*
recognition, pp. 3606–3613, 2014.
- 574
575 Carlos A Coello Coello and Nareli Cruz Cortés. Solving multiobjective optimization problems using
576 an artificial immune system. *Genetic programming and evolvable machines*, 6:163–190, 2005.
- 577
578 Haotian Cui, Chloe Wang, Hassaan Maan, Kuan Pang, Fengning Luo, Nan Duan, and Bo Wang.
579 scgpt: toward building a foundation model for single-cell multi-omics using generative ai. *Nature*
Methods, pp. 1–11, 2024.
- 580
581 Nico Daheim, Thomas Möllenhoff, Edoardo Ponti, Iryna Gurevych, and Mohammad Emtiyaz
582 Khan. Model merging by uncertainty-based gradient matching. In *The Twelfth International*
583 *Conference on Learning Representations*, 2024. URL [https://openreview.net/forum?](https://openreview.net/forum?id=D7KJmfEDQP)
584 [id=D7KJmfEDQP](https://openreview.net/forum?id=D7KJmfEDQP).
- 585
586 Kalyanmoy Deb and Himanshu Jain. An evolutionary many-objective optimization algorithm
587 using reference-point-based nondominated sorting approach, part i: solving problems with box
constraints. *IEEE transactions on evolutionary computation*, 18(4):577–601, 2013.
- 588
589 Kalyanmoy Deb, Manikanth Mohan, and Shikhar Mishra. Towards a quick computation of well-
590 spread pareto-optimal solutions. In *Evolutionary Multi-Criterion Optimization: Second Interna-*
591 *tional Conference, EMO 2003, Faro, Portugal, April 8–11, 2003. Proceedings 2*, pp. 222–236.
Springer, 2003.
- 592
593 Pala Tej Deep, Rishabh Bhardwaj, and Soujanya Poria. Della-merging: Reducing interference in
model merging through magnitude-based sampling. *arXiv preprint arXiv: 2406.11617*, 2024.

- 594 Alexey Dosovitskiy, Lucas Beyer, Alexander Kolesnikov, Dirk Weissenborn, Xiaohua Zhai, Thomas
595 Unterthiner, Mostafa Dehghani, Matthias Minderer, Georg Heigold, Sylvain Gelly, et al. An
596 image is worth 16x16 words: Transformers for image recognition at scale. *arXiv preprint*
597 *arXiv:2010.11929*, 2020.
- 598 Guodong Du, Jing Li, Hanqing Liu, Runhua Jiang, Shuyang Yu, Yifei Guo, S. Goh, and Ho-Kin Tang.
599 Knowledge fusion by evolving weights of language models. *Annual Meeting of the Association for*
600 *Computational Linguistics*, 2024. doi: 10.48550/arXiv.2406.12208.
- 601 Simon Du, Jason Lee, Haochuan Li, Liwei Wang, and Xiyu Zhai. Gradient descent finds global
602 minima of deep neural networks. In *International conference on machine learning*, pp. 1675–1685.
603 PMLR, 2019.
- 604 Saeed Ghadimi and Guanghui Lan. Stochastic first-and zeroth-order methods for nonconvex stochastic
605 programming. *SIAM journal on optimization*, 23(4):2341–2368, 2013.
- 606 Kaiming He, Xiangyu Zhang, Shaoqing Ren, and Jian Sun. Deep residual learning for image
607 recognition. In *Proceedings of the IEEE conference on computer vision and pattern recognition*,
608 pp. 770–778, 2016.
- 609 Patrick Helber, Benjamin Bischke, Andreas Dengel, and Damian Borth. Eurosat: A novel dataset
610 and deep learning benchmark for land use and land cover classification. *IEEE Journal of Selected*
611 *Topics in Applied Earth Observations and Remote Sensing*, 12(7):2217–2226, 2019.
- 612 Jordan Hoffmann, Sebastian Borgeaud, Arthur Mensch, Elena Buchatskaya, Trevor Cai, Eliza
613 Rutherford, Diego de Las Casas, Lisa Anne Hendricks, Johannes Welbl, Aidan Clark, et al.
614 Training compute-optimal large language models. *arXiv preprint arXiv:2203.15556*, 2022.
- 615 Evan J Hughes. Evolutionary many-objective optimisation: many once or one many? In *2005 IEEE*
616 *congress on evolutionary computation*, volume 1, pp. 222–227. IEEE, 2005.
- 617 Gabriel Ilharco, Marco Tulio Ribeiro, Mitchell Wortsman, Suchin Gururangan, Ludwig Schmidt,
618 Hannaneh Hajishirzi, and Ali Farhadi. Editing models with task arithmetic. *arXiv preprint*
619 *arXiv:2212.04089*, 2022.
- 620 Gabriel Ilharco, Marco Túlio Ribeiro, Mitchell Wortsman, Ludwig Schmidt, Hannaneh Hajishirzi,
621 and Ali Farhadi. Editing models with task arithmetic. In *The Eleventh International Conference*
622 *on Learning Representations, ICLR 2023, Kigali, Rwanda, May 1-5, 2023*. OpenReview.net, 2023.
623 URL <https://openreview.net/pdf?id=6t0Kwf8-jrj>.
- 624 Moksh Jain, Emmanuel Bengio, Alex Hernández-García, Jarrid Rector-Brooks, Bonaventure F. P.
625 Dossou, Chanakya Ajit Ekbote, Jie Fu, Tianyu Zhang, Michael Kilgour, Dinghuai Zhang, Lena
626 Simine, Payel Das, and Yoshua Bengio. Biological sequence design with gflownets. In Kamalika
627 Chaudhuri, Stefanie Jegelka, Le Song, Csaba Szepesvári, Gang Niu, and Sivan Sabato (eds.),
628 *International Conference on Machine Learning, ICML 2022, 17-23 July 2022, Baltimore, Maryland,*
629 *USA*, volume 162 of *Proceedings of Machine Learning Research*, pp. 9786–9801. PMLR, 2022.
630 URL <https://proceedings.mlr.press/v162/jain22a.html>.
- 631 Joel Jang, Seungone Kim, Bill Yuchen Lin, Yizhong Wang, Jack Hessel, Luke Zettlemoyer, Hannaneh
632 Hajishirzi, Yejin Choi, and Prithviraj Ammanabrolu. Personalized soups: Personalized large
633 language model alignment via post-hoc parameter merging. *arXiv preprint arXiv: 2310.11564*,
634 2023.
- 635 Albert Q. Jiang, Alexandre Sablayrolles, Antoine Roux, Arthur Mensch, Blanche Savary, Chris
636 Bamford, Devendra Singh Chaplot, Diego de las Casas, Emma Bou Hanna, Florian Bressand,
637 Gianna Lengyel, Guillaume Bour, Guillaume Lample, Léo Renard Lavaud, Lucile Saulnier, Marie-
638 Anne Lachaux, Pierre Stock, Sandeep Subramanian, Sophia Yang, Szymon Antoniak, Teven Le
639 Scao, Théophile Gervet, Thibaut Lavril, Thomas Wang, Timothée Lacroix, and William El Sayed.
640 Mixtral of experts. *arXiv preprint arXiv: 2401.04088*, 2024.
- 641 Xisen Jin, Xiang Ren, Daniel Preotiuc-Pietro, and Pengxiang Cheng. Dataless knowledge fusion
642 by merging weights of language models. In *The Eleventh International Conference on Learning*
643 *Representations, ICLR 2023, Kigali, Rwanda, May 1-5, 2023*. OpenReview.net, 2023. URL
644 <https://openreview.net/forum?id=FCnohuR6AnM>.

- 648 Jared Kaplan, Sam McCandlish, Tom Henighan, Tom B Brown, Benjamin Chess, Rewon Child, Scott
649 Gray, Alec Radford, Jeffrey Wu, and Dario Amodei. Scaling laws for neural language models.
650 *arXiv preprint arXiv:2001.08361*, 2020.
- 651 Jonathan Krause, Michael Stark, Jia Deng, and Li Fei-Fei. 3d object representations for fine-grained
652 categorization. In *Proceedings of the IEEE international conference on computer vision workshops*,
653 pp. 554–561, 2013.
- 654 Alex Krizhevsky, Geoffrey Hinton, et al. Learning multiple layers of features from tiny images. 2009.
- 655 Yann LeCun. The mnist database of handwritten digits. <http://yann.lecun.com/exdb/mnist/>, 1998.
- 656
657
658 Bingdong Li, Zixiang Di, Yanting Yang, Hong Qian, Peng Yang, Hao Hao, Ke Tang, and Aimin Zhou.
659 It’s morphing time: Unleashing the potential of multiple llms via multi-objective optimization.
660 *arXiv preprint arXiv: 2407.00487*, 2024.
- 661 Xi Lin, Hui-Ling Zhen, Zhenhua Li, Qing-Fu Zhang, and Sam Kwong. Pareto multi-task learning.
662 *Advances in neural information processing systems*, 32, 2019.
- 663
664 Xi Lin, Zhiyuan Yang, Qingfu Zhang, and Sam Kwong. Controllable pareto multi-task learning.
665 *arXiv preprint arXiv: 2010.06313*, 2020.
- 666
667 Michael S Matena and Colin A Raffel. Merging models with fisher-weighted averaging. *Advances in*
668 *Neural Information Processing Systems*, 35:17703–17716, 2022.
- 669
670 Sam McCandlish, Jared Kaplan, Dario Amodei, and OpenAI Dota Team. An empirical model of
671 large-batch training. *arXiv preprint arXiv:1812.06162*, 2018.
- 672
673 Henry B. Moss, David S. Leslie, Daniel Beck, Javier Gonzalez, and Paul Rayson. Boss:
674 Bayesian optimization over string spaces. In *Advances in Neural Information Process-*
675 *ing Systems*, 2020. URL [https://proceedings.neurips.cc/paper/2020/hash/](https://proceedings.neurips.cc/paper/2020/hash/b19aa25ff58940d974234b48391b9549-Abstract.html)
676 [b19aa25ff58940d974234b48391b9549-Abstract.html](https://proceedings.neurips.cc/paper/2020/hash/b19aa25ff58940d974234b48391b9549-Abstract.html).
- 677 Aviv Navon, Aviv Shamsian, Gal Chechik, and Ethan Fetaya. Learning the pareto front with
678 hypernetworks. *arXiv preprint arXiv: 2010.04104*, 2020.
- 679
680 Yuval Netzer, Tao Wang, Adam Coates, Alessandro Bissacco, Baolin Wu, Andrew Y Ng, et al.
681 Reading digits in natural images with unsupervised feature learning. In *NIPS workshop on deep*
682 *learning and unsupervised feature learning*, volume 2011, pp. 7. Granada, Spain, 2011.
- 683 Maria-Elena Nilsback and Andrew Zisserman. Automated flower classification over a large number
684 of classes. In *2008 Sixth Indian conference on computer vision, graphics & image processing*, pp.
685 722–729. IEEE, 2008.
- 686
687 National Institutes of Health et al. Nih clinical center provides one of the largest publicly available
688 chest x-ray datasets to scientific community, 2017.
- 689
690 Guillermo Ortiz-Jiménez, Alessandro Favero, and P. Frossard. Task arithmetic in the tangent space:
691 Improved editing of pre-trained models. *Neural Information Processing Systems*, 2023. doi:
692 10.48550/arXiv.2305.12827.
- 693
694 E. O. Pyzer-Knapp. Bayesian optimization for accelerated drug discovery. *IBM Journal of Research*
695 *and Development*, 62(6):2:1–2:7, 2018. doi: 10.1147/JRD.2018.2881731.
- 696
697 Alec Radford, Jong Wook Kim, Chris Hallacy, Aditya Ramesh, Gabriel Goh, Sandhini Agarwal,
698 Girish Sastry, Amanda Askell, Pamela Mishkin, Jack Clark, et al. Learning transferable visual
699 models from natural language supervision. In *International conference on machine learning*, pp.
700 8748–8763. PMLR, 2021.
- 701 Alexandre Ram’e, Nino Vieillard, L’eonard Hussenot, Robert Dadashi, Geoffrey Cideron, Olivier
Bachem, and Johan Ferret. Warm: On the benefits of weight averaged reward models. *International
Conference on Machine Learning*, 2024. doi: 10.48550/arXiv.2401.12187.

- 702 Alexandre Ramé, Guillaume Couairon, Mustafa Shukor, Corentin Dancette, Jean-Baptiste Gaya,
703 L. Soulier, and M. Cord. Rewarded soups: towards pareto-optimal alignment by interpolating
704 weights fine-tuned on diverse rewards. *Neural Information Processing Systems*, 2023. doi:
705 10.48550/arXiv.2306.04488.
- 706
707 Alexandre Ramé, Johan Ferret, Nino Vieillard, Robert Dadashi, Léonard Hussenot, Pierre-Louis
708 Cedoz, Pier Giuseppe Sessa, Sertan Girgin, Arthur Douillard, and Olivier Bachem. Warp: On the
709 benefits of weight averaged rewarded policies. *arXiv preprint arXiv: 2406.16768*, 2024.
- 710
711 Baptiste Rozière, Jonas Gehring, Fabian Gloeckle, Sten Sootla, Itai Gat, Xiaoqing Ellen Tan, Yossi
712 Adi, Jingyu Liu, Romain Sauvestre, Tal Remez, Jérémy Rapin, Artyom Kozhevnikov, Ivan Evtimov,
713 Joanna Bitton, Manish Bhatt, Cristian Canton Ferrer, Aaron Grattafiori, Wenhan Xiong, Alexandre
714 Défossez, Jade Copet, Faisal Azhar, Hugo Touvron, Louis Martin, Nicolas Usunier, Thomas
715 Scialom, and Gabriel Synnaeve. Code llama: Open foundation models for code. *arXiv preprint
716 arXiv: 2308.12950*, 2023.
- 717
718 Michael Ruchte and Josif Grabocka. Scalable pareto front approximation for deep multi-objective
719 learning. *2021 IEEE International Conference on Data Mining (ICDM)*, pp. 1306–1311, 2021.
doi: 10.1109/ICDM51629.2021.00162.
- 720
721 Ozan Sener and Vladlen Koltun. Multi-task learning as multi-objective optimization. In
722 S. Bengio, H. Wallach, H. Larochelle, K. Grauman, N. Cesa-Bianchi, and R. Garnett (eds.),
723 *Advances in Neural Information Processing Systems*, volume 31. Curran Associates, Inc.,
724 2018. URL [https://proceedings.neurips.cc/paper_files/paper/2018/
file/432aca3a1e345e339f35a30c8f65edce-Paper.pdf](https://proceedings.neurips.cc/paper_files/paper/2018/file/432aca3a1e345e339f35a30c8f65edce-Paper.pdf).
- 725
726 Ken Shoemake. Animating rotation with quaternion curves. In *Proceedings of the 12th Annual
727 Conference on Computer Graphics and Interactive Techniques, SIGGRAPH ’85*, pp. 245–254,
728 New York, NY, USA, 1985. Association for Computing Machinery. ISBN 0897911660. doi:
729 10.1145/325334.325242. URL <https://doi.org/10.1145/325334.325242>.
- 730
731 Johannes Stallkamp, Marc Schlipsing, Jan Salmen, and Christian Igel. The german traffic sign
732 recognition benchmark: a multi-class classification competition. In *The 2011 international joint
733 conference on neural networks*, pp. 1453–1460. IEEE, 2011.
- 734
735 Hui Su, Zhi Tian, Xiaoyu Shen, and Xunliang Cai. Unraveling the mystery of scaling laws: Part i.
736 *arXiv preprint arXiv:2403.06563*, 2024.
- 737
738 Kei Terayama, Masato Sumita, Ryo Tamura, and Koji Tsuda. Black-box optimization for automated
739 discovery. *Accounts of Chemical Research*, 54(6):1334–1346, 2021.
- 740
741 Arun James Thirunavukarasu, Darren Shu Jeng Ting, Kabilan Elangovan, Laura Gutierrez, Ting Fang
742 Tan, and Daniel Shu Wei Ting. Large language models in medicine. *Nature medicine*, 29(8):
743 1930–1940, 2023.
- 744
745 Hugo Touvron, Louis Martin, Kevin Stone, Peter Albert, Amjad Almahairi, Yasmine Babaei, Nikolay
746 Bashlykov, Soumya Batra, Prajjwal Bhargava, Shruti Bhosale, Dan Bikel, Lukas Blecher, Cris-
747 tian Canton Ferrer, Moya Chen, Guillem Cucurull, David Esiobu, Jude Fernandes, Jeremy Fu,
748 Wenyin Fu, Brian Fuller, Cynthia Gao, Vedanuj Goswami, Naman Goyal, Anthony Hartshorn,
749 Saghar Hosseini, Rui Hou, Hakan Inan, Marcin Kardas, Viktor Kerkez, Madian Khabsa, Isabel
750 Kloumann, Artem Korenev, Punit Singh Koura, Marie-Anne Lachaux, Thibaut Lavril, Jenya Lee,
751 Diana Liskovich, Yinghai Lu, Yuning Mao, Xavier Martinet, Todor Mihaylov, Pushkar Mishra,
752 Igor Molybog, Yixin Nie, Andrew Poulton, Jeremy Reizenstein, Rashi Rungta, Kalyan Saladi,
753 Alan Schelten, Ruan Silva, Eric Michael Smith, Ranjan Subramanian, Xiaoqing Ellen Tan, Binh
754 Tang, Ross Taylor, Adina Williams, Jian Xiang Kuan, Puxin Xu, Zheng Yan, Iliyan Zarov, Yuchen
755 Zhang, Angela Fan, Melanie Kambadur, Sharan Narang, Aurelien Rodriguez, Robert Stojnic,
Sergey Edunov, and Thomas Scialom. Llama 2: Open foundation and fine-tuned chat models.
arXiv preprint arXiv: 2307.09288, 2023.
- David Allen Van Veldhuizen. *Multiobjective evolutionary algorithms: classifications, analyses, and
new innovations*. Air Force Institute of Technology, 1999.

- 756 Haoxiang Wang, Yong Lin, Wei Xiong, Rui Yang, Shizhe Diao, Shuang Qiu, Han Zhao, and Tong
757 Zhang. Arithmetic control of llms for diverse user preferences: Directional preference alignment
758 with multi-objective rewards. *arXiv preprint arXiv: 2402.18571*, 2024.
759
- 760 Xiaosong Wang, Yifan Peng, Le Lu, Zhiyong Lu, Mohammadhadi Bagheri, and Ronald M Summers.
761 Chestx-ray8: Hospital-scale chest x-ray database and benchmarks on weakly-supervised classi-
762 fication and localization of common thorax diseases. In *Proceedings of the IEEE conference on*
763 *computer vision and pattern recognition*, 2017.
- 764 James T. Wilson, Riccardo Moriconi, Frank Hutter, and Marc Peter Deisenroth. The reparameteriza-
765 tion trick for acquisition functions, 2017.
766
- 767 Michael Wornow, Rahul Thapa, Ethan Steinberg, Jason Fries, and Nigam Shah. Ehrshot: An ehr
768 benchmark for few-shot evaluation of foundation models. 2023.
- 769 Mitchell Wortsman, Gabriel Ilharco, S. Gadre, R. Roelofs, Raphael Gontijo-Lopes, Ari S. Morcos,
770 Hongseok Namkoong, Ali Farhadi, Y. Carmon, Simon Kornblith, and Ludwig Schmidt. Model
771 soups: averaging weights of multiple fine-tuned models improves accuracy without increasing
772 inference time. *International Conference on Machine Learning*, 2022a. doi: 10.48550/arXiv.2203.
773 05482.
- 774 Mitchell Wortsman, Gabriel Ilharco, Jong Wook Kim, Mike Li, Simon Kornblith, Rebecca Roelofs,
775 Raphael Gontijo Lopes, Hannaneh Hajishirzi, Ali Farhadi, Hongseok Namkoong, et al. Robust
776 fine-tuning of zero-shot models. In *Proceedings of the IEEE/CVF conference on computer vision*
777 *and pattern recognition*, pp. 7959–7971, 2022b.
778
- 779 Yusong Wu, Ke Chen, Tianyu Zhang, Yuchen Hui, Taylor Berg-Kirkpatrick, and Shlomo Dubnov.
780 Large-scale contrastive language-audio pretraining with feature fusion and keyword-to-caption aug-
781 mentation. In *IEEE International Conference on Acoustics, Speech and Signal Processing ICASSP*
782 *2023, Rhodes Island, Greece, June 4-10, 2023*, pp. 1–5. IEEE, 2023. doi: 10.1109/ICASSP49357.
783 2023.10095969. URL <https://doi.org/10.1109/ICASSP49357.2023.10095969>.
- 784 Jianxiong Xiao, Krista A Ehinger, James Hays, Antonio Torralba, and Aude Oliva. Sun database:
785 Exploring a large collection of scene categories. *International Journal of Computer Vision*, 119:
786 3–22, 2016.
787
- 788 Prateek Yadav, Derek Tam, Leshem Choshen, Colin Raffel, and Mohit Bansal. Ties-merging:
789 Resolving interference when merging models. *Neural Information Processing Systems*, 2023.
- 790 Prateek Yadav, Derek Tam, Leshem Choshen, Colin A Raffel, and Mohit Bansal. Ties-merging:
791 Resolving interference when merging models. *Advances in Neural Information Processing Systems*,
792 36, 2024.
793
- 794 Enneng Yang, Zhenyi Wang, Li Shen, Shiwei Liu, Guibing Guo, Xingwei Wang, and Dacheng Tao.
795 Adamerging: Adaptive model merging for multi-task learning. *arXiv preprint arXiv:2310.02575*,
796 2023.
- 797 Enneng Yang, Zhenyi Wang, Li Shen, Shiwei Liu, Guibing Guo, Xingwei Wang, and Dacheng
798 Tao. Adamerging: Adaptive model merging for multi-task learning. In *The Twelfth International*
799 *Conference on Learning Representations*, 2024. URL [https://openreview.net/forum?](https://openreview.net/forum?id=nZP6NgD3QY)
800 [id=nZP6NgD3QY](https://openreview.net/forum?id=nZP6NgD3QY).
801
- 802 Le Yu, Bowen Yu, Haiyang Yu, Fei Huang, and Yongbin Li. Language models are super mario:
803 Absorbing abilities from homologous models as a free lunch. *arXiv preprint arXiv:2311.03099*,
804 2023.
- 805 Xiaohua Zhai, Basil Mustafa, Alexander Kolesnikov, and Lucas Beyer. Sigmoid loss for language
806 image pre-training. *IEEE International Conference on Computer Vision*, 2023. doi: 10.1109/
807 ICCV51070.2023.01100.
- 808
- 809 Qingfu Zhang and Hui Li. Moea/d: A multiobjective evolutionary algorithm based on decomposition.
IEEE Transactions on evolutionary computation, 11(6):712–731, 2007.

810 Yifan Zhong, Chengdong Ma, Xiaoyuan Zhang, Ziran Yang, Haojun Chen, Qingfu Zhang, Siyuan Qi,
811 and Yaodong Yang. Panacea: Pareto alignment via preference adaptation for llms. *arXiv preprint*
812 *arXiv: 2402.02030*, 2024.

813
814 Zhanhui Zhou, Jie Liu, Chao Yang, Jing Shao, Yu Liu, Xiangyu Yue, Wanli Ouyang, and Yu Qiao.
815 Beyond one-preference-fits-all alignment: Multi-objective direct preference optimization. *arXiv*
816 *preprint arXiv: 2310.03708*, 2023.

817
818
819
820
821
822
823
824
825
826
827
828
829
830
831
832
833
834
835
836
837
838
839
840
841
842
843
844
845
846
847
848
849
850
851
852
853
854
855
856
857
858
859
860
861
862
863

864	Contents	
865		
866	A Notations	18
867		
868	B More Discussion on Related Work	18
869		
870	C Additional Details on the Methods	19
871	C.1 Proof: Negligibility of the Remainder in Multivariate Taylor Series	19
872	C.2 Closed-form Solution for Surrogate Model Parameters	20
873		
874	D Additional Details on Experiments	21
875	D.1 Experiment setup	21
876	D.2 Additional metric: Generational distance and inverted generational distance	21
877	D.3 Zero-shot Medical Image Classification	22
878	D.4 Merging Language Model	22
879	D.5 Additional experiment results on ResNet	24
880		
881	E More Details on Algorithms	25
882	E.1 Plain LocMAP	25
883	E.2 Nested-Merging LocMAP	25
884	E.2.1 Overview	25
885	E.2.2 Time Complexity of Nested-Merging LocMAP	25
886	E.2.3 Intermediate Pareto Fronts in Each Round	26
887	E.2.4 Results on using nested merging to merge 8 models	27
888	E.3 Bayesian LocMAP	28
889	E.3.1 Performance of Bayesian LocMAP	28
890		
891	F Potential Q & A	31
892	F.1 The authors assume a setting where it is computationally expensive to query the model evaluations. But is this the reality?	31
893	F.2 How is LocMAP different from other MOOP methods, such as linear scalarization?	31
894	F.3 Why does quadratic approximation have a lower cost?	31
895	F.4 Why not compare to Git-Rebasin Ainsworth et al. (2023)?	31
896	F.5 Why does nested-merging LocMAP not give a complete Pareto front?	32
897	F.6 It seems nested-merging LocMAP performs worse than LocMAP. What is the mean- ing of it?	32
898	F.7 Why does nested-merging LocMAP not output the optimal solution?	32
899	F.8 How do you deal with gradient and Hessian in the second-order Taylor expansion?	32
900		
901		
902		
903		
904		
905		
906		
907		
908		
909		
910		
911		
912		
913		
914		
915		
916		
917		

A NOTATIONS

For aid of readability, we provide the table of notations in Table 5.

Table 5: Table of notations.

Notations	Explanation
N	Number of tasks
\mathbf{c}	Vector of scaling coefficients for task vectors
c_n	Scaling coefficients for the n th task
θ_{pre}	Pretrained model parameters
$\theta_m(\mathbf{c})$	Merged model parameters as a function of scaling vector \mathbf{c}
\mathbf{v}_n	Task vector for task n
\mathbf{V}	Task matrix formed by concatenating task vectors
$M_n(\mathbf{c})$	Evaluation metric for task n as a function of \mathbf{c}
\mathbf{A}_n	Quadratic coefficient matrix in the surrogate model
\mathbf{b}_n	Linear coefficient vector in the surrogate model
e_n	Constant term in the surrogate model
$\tilde{M}_n(\mathbf{c}; \mathbf{A}_n, \mathbf{b}_n, e_n)$	Surrogate quadratic model for task n
Ω	Set of scaling coefficient vectors \mathbf{c} used for estimating surrogate model parameters
K	Number of sampled coefficient vectors in set Ω

B MORE DISCUSSION ON RELATED WORK

Second-order Taylor expansion In deep learning, the second-order Taylor expansion and thus the quadratic approximation on the evaluation metric is an important technique, that characterizes the metric landscape. For example, the Newton-Ralphson method is derived from it: $\mathbf{w}_t - \mathbf{w}_{t+1} = \mathbf{H}^{-1}\mathbf{G} = \text{argmin}_{\mathbf{v}} M(\mathbf{w}_t - \mathbf{v})$ given that $M(\mathbf{w}_t - \mathbf{v}) = M(\mathbf{w}_t) - \mathbf{v}\mathbf{G} + \frac{1}{2}\mathbf{v}^{\top}\mathbf{H}\mathbf{v}$. The quadratic approximation is also combined with Lipschitz smoothness (L) in the classic convergence analysis of SGD Bubeck et al. (2015); Ghadimi & Lan (2013), through $M(\mathbf{w}_t - \eta\mathbf{G}) \leq M(\mathbf{w}_t) - \eta\|\mathbf{G}\|^2 + \frac{L\eta^2}{2}\|\mathbf{G}\|^2$. Interestingly, although the approximation is only accurate in the local neighborhood, it can be used to indicate the global convergence over the iterations. One reason is that state-of-the-art neural networks are usually over-parameterized and undergo lazy training, meaning that the converging parameters are close to the initialization Chizat et al. (2019); Du et al. (2019); Allen-Zhu et al. (2019). Thus, the local approximation informs the global convergence behavior. In particular, this approximation has played important roles in the scaling laws of neural networks (e.g. Equation 3.3 in Su et al. (2024)) that predict the performance and help select hyperparameters before training actually takes place.

Pareto fronts for Multi-task Learning Recent advancements in multi-task learning (MTL) have seen diverse approaches to Pareto Front learning in machine learning. Sener & Koltun (2018) explicitly formulated multi-task learning as a multi-objective optimization problem and adapted gradient-based multi-objective optimization algorithms to large-scale learning problems. Lin et al. (2019) developed a constrained optimization approach to find multiple Pareto optimal solutions representing different trade-offs among tasks in multi-task learning and solved decomposed sub-problems in parallel using gradient-based optimization. It requires separate training runs for each solution. Navon et al. (2020) and Lin et al. (2020) employed hypernetworks for continuous Pareto Front approximation, generating target network weights based on preferred trade-offs. However, the size of these hypernetworks can become prohibitively large and needs to be properly trained as well. Ruchte and Grabocka Ruchte & Grabocka (2021) introduced a memory-efficient method by augmenting network inputs with desired trade-offs, although this may obscure the network’s conditioning due to nonlinear dynamics, and it is also based on the gradient updating method.

Model-merging Applications in LLM In the realm of model merging applications for language model preferences, recent research has made significant progress. Ramé et al. (2023) and Jang et al. (2023) introduced “rewarded soups” and “personalized soups”, which utilize model soup to

interpolate weights of networks fine-tuned on diverse rewards to achieve Pareto-optimal generalization across preference spaces and address the challenge of aligning large language models with individual perspectives. WARP (Weight Averaged Rewarded Policies) Ramé et al. (2024) and WARM (Weight Averaged Reward Models) Ramé et al. (2024) demonstrate how merging policies or reward models in weight space can refine the trade-off between competing constraints, such as reward optimization and alignment with pre-trained knowledge or human preferences. Zhong et al. (2024) developed “Panacea”, which reframes alignment as a multi-dimensional preference optimization problem, using singular value decomposition-based low-rank adaptation to guide model behavior with a low-dimensional preference vector. To address the limitations of scalar rewards in RLHF, Zhou et al. (2023) introduced Multi-Objective Direct Preference Optimization, an RL-free algorithm that extends Direct Preference Optimization to handle multiple alignment objectives efficiently. Du et al. (2024) relies on “mutation” and crossover operations typical of evolutionary algorithms, exploring the parameter space by combining and perturbing existing solutions. Models are evaluated on development datasets, and only those that improve upon their predecessors are retained, guiding the population toward better-performing solutions. Li et al. (2024) employs Bayesian optimization with a weak-to-strong approach and utilizes Fisher information to improve the selection of configurations for evaluation, aiming to find optimal merging configurations within limited computational budgets. Finally, Wang et al. (2024) proposed the Directional Preference Alignment framework, which incorporates multi-objective reward modeling to represent user preferences, offering intuitive arithmetic control over LLM generation for diverse user preferences.

Bayesian Optimization Bayesian optimization has been widely used in scenarios that require efficient exploration of parameter spaces, particularly when evaluating the performance of each configuration is costly or time-consuming. This method is especially advantageous in machine learning and hyperparameter tuning, where traditional optimization techniques may be computationally prohibitive. Popular Bayesian optimization methods and applications are Wilson et al. (2017); Jain et al. (2022); Moss et al. (2020); Pyzer-Knapp (2018); Terayama et al. (2021).

C ADDITIONAL DETAILS ON THE METHODS

C.1 PROOF: NEGLIGIBILITY OF THE REMAINDER IN MULTIVARIATE TAYLOR SERIES

Corollary 2. *If $f : \mathbb{R}^n \rightarrow \mathbb{R}$ is $(k + 1)$ times continuously differentiable in a neighborhood around a point $a \in \mathbb{R}^n$, then the Taylor polynomial $T_k(x)$ of order k provides an accurate approximation of $f(x)$ when x is sufficiently close to a . Furthermore, the remainder term $R_k(x)$ becomes negligibly small as $\|x - a\|$ approaches zero, assuming that the $(k + 1)$ th derivatives of f are bounded by a constant M in the neighborhood between a and x .*

Proof Consider the Taylor series expansion of f around the point a , truncated at order k :

$$T_k(x) = \sum_{|\alpha| \leq k} \frac{D^\alpha f(a)}{\alpha!} (x - a)^\alpha$$

where α is a multi-index of non-negative integers, $D^\alpha f(a)$ denotes the partial derivatives of f at a corresponding to α , and $(x - a)^\alpha = (x_1 - a_1)^{\alpha_1} \dots (x_n - a_n)^{\alpha_n}$.

Assumptions

1. *Proximity:* $\|x - a\| \rightarrow 0$ where $\|\cdot\|$ denotes the Euclidean norm in \mathbb{R}^n .
2. *Bounded Derivatives:* There exists a constant M such that for all multi-indices α with $|\alpha| \equiv k + 1$, the norm of the tensor $D^\alpha f$ evaluated at any point ξ between a and x is bounded by M .

$$\|D^\alpha f(\xi)\| = \sup_{\|v_1\|=1, \dots, \|v_{k+1}\|=1} |D^\alpha f(\xi)(v_1, \dots, v_{k+1})| \leq M$$

The remainder term of the Taylor series expansion is given by:

$$R_k(x) = \sum_{|\alpha|=k+1} \frac{D^\alpha f(\xi)}{\alpha!} (x-a)^\alpha$$

Given the assumptions, we estimate:

$$|R_k(x)| \leq \sum_{|\alpha|=k+1} \frac{\|D^\alpha f(\xi)\|}{\alpha!} \|x-a\|^{k+1} \leq \sum_{|\alpha|=k+1} \frac{M}{\alpha!} \|x-a\|^{k+1}$$

As $\|x-a\| \rightarrow 0$, the term $\|x-a\|^{k+1}$ goes to zero. Thus, the remainder term $R_k(x)$ becomes arbitrarily small, making it negligible.

In conclusion, under the stated assumptions, the Taylor series truncated at order k , $T_k(x)$, provides an accurate approximation of $f(x)$ near a , and the remainder $R_k(x)$ can be ignored as $\|x-a\| \rightarrow 0$ and the higher-order derivatives remain bounded by M .

C.2 CLOSED-FORM SOLUTION FOR SURROGATE MODEL PARAMETERS

Corollary 3 (Closed-form Solution for Surrogate Model Parameters). *Under Assumption 1, for each task $n = 1, \dots, N$, the optimization problem*

$$(A_n^*, \mathbf{b}_n^*, e_n^*) = \arg \min_{A_n, \mathbf{b}_n, e_n} \sum_{\mathbf{c} \in \Omega} \left| M_n(\theta_m(\mathbf{c})) - \tilde{M}_n(\mathbf{c}; A_n, \mathbf{b}_n, e_n) \right|^2$$

is equivalent to solving the following linear regression problem:

1. **Predictors:** For each coefficient vector $\mathbf{c} = (c_1, c_2, \dots, c_N)^\top \in \mathbb{R}^N$, construct the predictor vector $\mathbf{C}_n(\mathbf{c}) \in \mathbb{R}^{\frac{N(N+3)}{2}+1}$ as

$$\mathbf{C}_n(\mathbf{c}) = [c_1^2, c_2^2, \dots, c_N^2, c_1c_2, c_1c_3, \dots, c_{N-1}c_N, c_1, c_2, \dots, c_N, 1]$$

This vector includes:

- Quadratic terms: c_i^2 for $i = 1, \dots, N$.
- Interaction terms: $c_i c_j$ for $1 \leq i < j \leq N$.
- Linear terms: c_i for $i = 1, \dots, N$.
- Constant term: 1.

2. **Response Variable:** Let $\mathbf{y}_n \in \mathbb{R}^K$ be the vector of observed evaluation metrics for task n across all sampled coefficients $\Omega = \{\mathbf{c}^{(1)}, \dots, \mathbf{c}^{(K)}\}$:

$$\mathbf{y}_n = \begin{bmatrix} M_n(\theta_m(\mathbf{c}^{(1)})) \\ M_n(\theta_m(\mathbf{c}^{(2)})) \\ \vdots \\ M_n(\theta_m(\mathbf{c}^{(K)})) \end{bmatrix}$$

3. **Design Matrix:** Construct the design matrix $\mathbf{C}_n \in \mathbb{R}^{K \times (\frac{N(N+3)}{2}+1)}$ where each row corresponds to $\mathbf{C}_n(\mathbf{c}^{(k)})^\top$ for $k = 1, \dots, K$.

4. **Coefficient Vector:** Define the coefficient vector $\beta_n \in \mathbb{R}^{\frac{N(N+3)}{2}+1}$ as

$$\beta_n = \begin{bmatrix} \text{vec}(A_n) \\ \mathbf{b}_n \\ e_n \end{bmatrix}$$

where $\text{vec}(A_n)$ represents the vectorization of the upper triangular part of A_n , including the diagonal elements.

Optimal Solution: The parameters $(A_n^*, \mathbf{b}_n^*, c_n^*)$ that minimize the mean squared error are obtained via the Ordinary Least Squares (OLS) solution:

$$\beta_n^* = (\mathbf{C}_n^\top \mathbf{C}_n)^{-1} \mathbf{C}_n^\top \mathbf{y}_n$$

Interpretation: This closed-form solution provides the optimal surrogate model parameters by fitting a quadratic model to the observed evaluation metrics through linear regression. The design matrix \mathbf{C}_n incorporates all necessary quadratic, interaction, linear, and constant terms, enabling the surrogate model $\tilde{M}_n(\mathbf{c}; A_n, \mathbf{b}_n, c_n)$ to accurately approximate $M_n(\theta_m(\mathbf{c}))$ within the specified region.

D ADDITIONAL DETAILS ON EXPERIMENTS

D.1 EXPERIMENT SETUP

Table 6: Experiment setup in terms of task details and models.

Task type	Metric	# of total tasks	Model type
Zero-shot Classification (normal)	Accuracy	8	ViT-B/32 (CLIP) (Dosovitskiy et al. (2020))
Zero-shot Classification (medical)	Accuracy	2	ViT-B/32 (CLIP) (Dosovitskiy et al. (2020))
Language Generation	Loss/Perplexity	4	Llama3-8B (Touvron et al. (2023))
Image Classification	Accuracy	3	ResNet-18 (He et al. (2016))

D.2 ADDITIONAL METRIC: GENERATIONAL DISTANCE AND INVERTED GENERATIONAL DISTANCE

We evaluated the quality of the Pareto front in capturing the shape of the ground truth Pareto front by measuring how much the predicted Pareto front converges to the ground truth Pareto front by calculating the generational distance (GD) Van Veldhuizen (1999) and how much the predicted Pareto front covers the ground truth Pareto front by calculating the inverted generational distance (IGD) Coello & Cortés (2005). GD and IGD are standard measures used in evolutionary multi-objective optimization to evaluate the solutions found by the evolutionary algorithms. Given two solution sets $PF_i = \{\tilde{M}_1^i(\theta_{merged}(\mathbf{c})), \dots, \tilde{M}_N^i(\theta_{merged}(\mathbf{c}))\}$, $i = 1, 2$, the GD and IGD metrics are defined as

$$GD(PF_1) \equiv \frac{1}{K} \left(\sum_{i=1}^K d_i^p \right)^{1/p} \quad \text{and} \quad IGD(PF_1) \equiv \frac{1}{M} \left(\sum_{i=1}^M \tilde{d}_i^p \right)^{1/p}$$

where d_i is the minimal Euclidean distance from $\tilde{M}_1^1(\theta_{merged}(\mathbf{c}))$ to PF_2 and \tilde{d}_i is the minimal Euclidean distance from $\tilde{M}_1^2(\theta_{merged}(\mathbf{c}))$ to PF_1 .

Since the Pareto front that resulted from the direct search method when the number of tasks is low (i.e. strictly smaller than 4) can be deemed as ground truth Pareto fronts, we calculated the GD and IGD between the Pareto fronts obtained by LocMAP and the brute force grid search method.

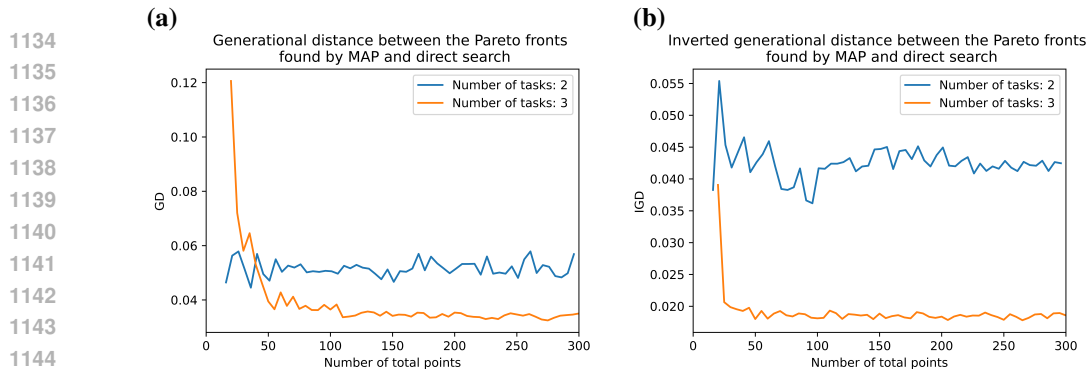


Figure 6: (a) Generational distance between the Pareto fronts by LocMAP and by direct search for dimensions 2 and 3. (b) Inverted generational distance between the Pareto fronts by LocMAP and by direct search for dimensions 2 and 3. For both subfigures, the x-axis is the number of total scaling coefficients used by LocMAP. For dimension 2, direct search used 200 scaling coefficients, and 300 for dimension 3.

D.3 ZERO-SHOT MEDICAL IMAGE CLASSIFICATION

In addition to natural images, we used another dataset consisting of over 112,000 chest X-rays and 30,000 unique patients of Health et al. (2017). It originally contained 15 classes (14 diseases and 1 class for no finding). We split the dataset into two groups, where medical task 1 specifically tries to classify Atelectasis, Consolidation, Infiltration, Pneumothorax, and medical task 2 tries to classify Nodule, Mass, and Hernia. An example image taken from the dataset is shown in Figure 7 (a).

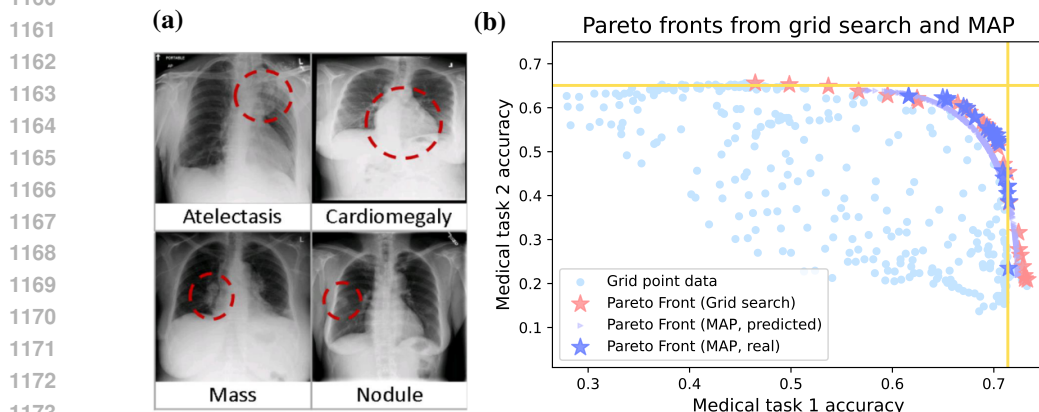


Figure 7: (a) Example figure from the NIH of Health et al. (2017) dataset. (b) Pareto fronts found by brute-force direct search using 400 points and by LocMAP using 30 points. We randomly sampled 25 points from the predicted Pareto front by LocMAP. The resulting IGD is 0.016, and GD is 0.014.

D.4 MERGING LANGUAGE MODEL

Merging Languages We merge Llama-3-8B language models in French³ and Arabic⁴, as well as Chinese⁵ and Japanese⁶, as shown in Table 7. The ground truth Pareto front, however, exhibits significant limitations. It contains only a sparse set of points, indicating that few merged models dominate the rest. This also suggests that the trade-off between metrics across different languages

³<https://huggingface.co/jpacifico/French-Alpaca-Llama3-8B-Instruct-v1.0>

⁴<https://huggingface.co/MohamedRashad/Arabic-Orpo-Llama-3-8B-Instruct>

⁵<https://huggingface.co/shenzhi-wang/Llama3-8B-Chinese-Chat>

⁶<https://huggingface.co/haqishen/Llama-3-8B-Japanese-Instruct>

is not substantial. Despite these challenges, our algorithm successfully identifies the Pareto fronts. Please refer to Table 7 and Appendix D.4 for GD and IGD metrics between the Pareto fronts find by Grid Search and find by LocMAP and a visualization of the Pareto fronts found by LocMAP.

Furthermore, we experimented with merging Arabic+French and Chinese+Japanese using the nested scheme described in Algorithm 2, while considering various preference settings. However, the resulting Pareto front typically contains only a single model. This sparsity hinders our ability to effectively characterize a meaningful Pareto front in such scenarios.

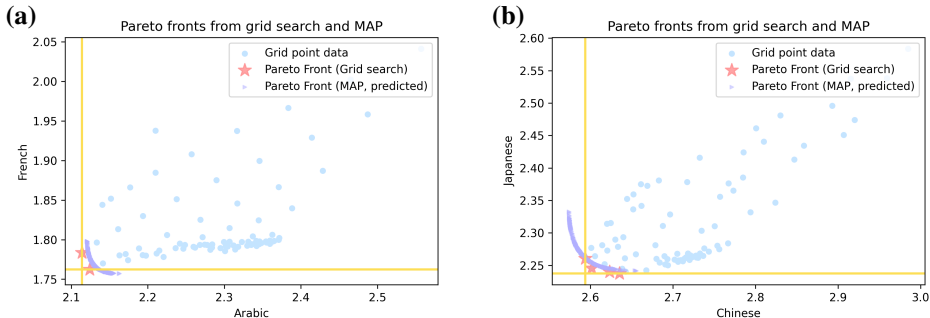


Figure 8: (a) Amortized Pareto front by LocMAP on merging Llama-3 fine-tuned on French with Llama-3 fine-tuned on Arabic; (b) Amortized Pareto front on merging Llama-3 fine-tuned on Chinese with Llama-3 fine-tuned on Japanese. The yellow line represents the evaluation metric of the corresponding single task model.

Merging Language Models Specializing in Math and Code Following DARE (Yu et al. (2023)), we also experimented with merging two language models each with 13B parameters specializing in mathematics (referred to as the math model) and coding (referred to as the code model). The base model used is Llama-2 13B⁷, the math model is WizardMath-13B⁸, and the code model is llama-2-13b-code-alpaca⁹. Both the math and code models are fine-tuned versions of Llama-2 13B.

The primary reason for selecting Llama-2 as the base model, rather than newer models like Llama-3 or Qwen-2.5, is the lack of suitable math and code models fine-tuned from the same base configuration. For instance, although Qwen-2.5 provides both Qwen-2.5-Math and Qwen-2.5-Coder, the two models differ significantly in their configurations, specifically, the rope theta parameter is set to 10,000.0 for the math model and 1,000,000.0 for the coder model. This discrepancy makes it challenging to effectively merge these models. Please refer to Figure 9 for a visualization of the Pareto front obtained from LocMAP and Table 7 for GD and IGD metrics between the Pareto fronts obtained from Grid Search and from LocMAP.

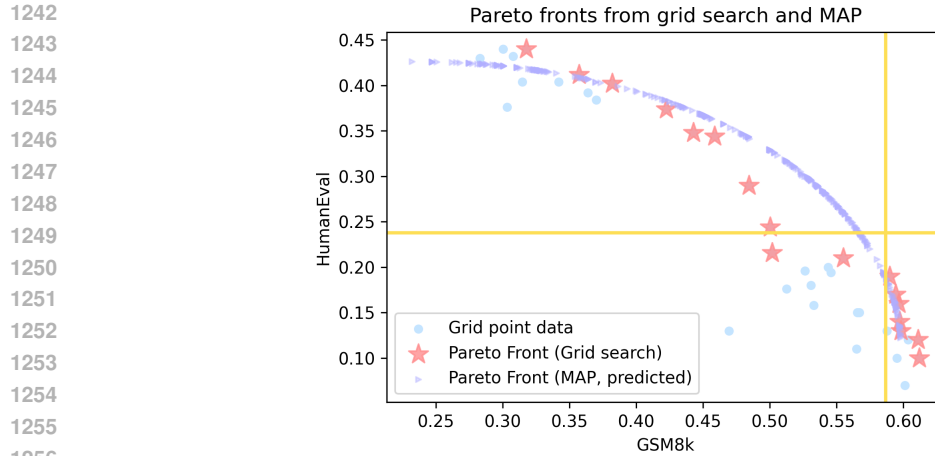
Table 7: The GD and IGD metrics score for Arabic+French, Chinese+Japanese and Math+Code between the Pareto fronts find by Grid Search and find by LocMAP.

	GD	IGD	GD+IGD
Arabic+French	0.023 _{0.010}	0.035 _{0.018}	0.058 _{0.028}
Chinese+Japanese	0.014 _{0.013}	0.028 _{0.017}	0.041 _{0.026}
Math+Code	0.039 _{0.009}	0.018 _{0.002}	0.057 _{0.008}

⁷<https://huggingface.co/meta-llama/Llama-2-13b-hf>

⁸<https://huggingface.co/vanillaOVO/WizardMath-13B-V1.0>

⁹<https://huggingface.co/layoric/llama-2-13b-code-alpaca>

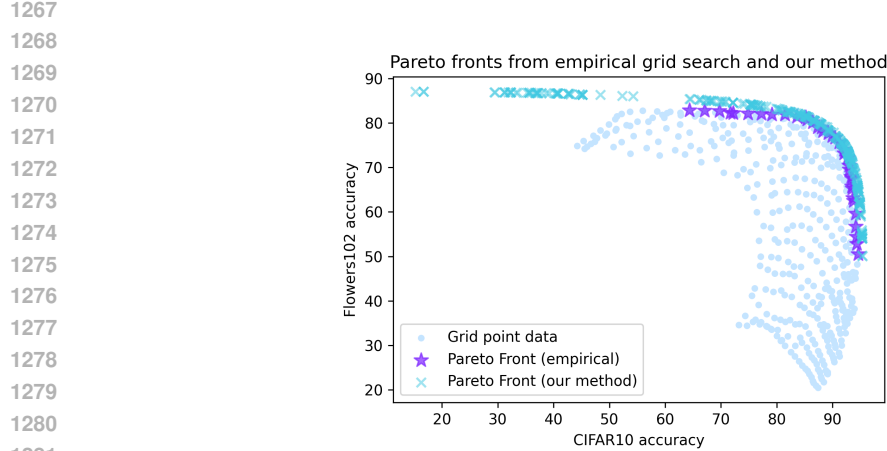


1257 Figure 9: Amortized Pareto front by LocMAP on merging WizardMath-13B and code-alpaca-13B.
 1258 The yellow line represents the evaluation metric of the corresponding single task model.

1260 D.5 ADDITIONAL EXPERIMENT RESULTS ON RESNET

1261

1262 We performed additional experiments on ResNet18 He et al. (2016) by merging two models finetuned
 1263 on CIFAR10 Krizhevsky et al. (2009) and Flowers102 Nilsback & Zisserman (2008) and show
 1264 the obtained Pareto front in Figure 10. Unlike ViT models, which perform zero-shot classification,
 1265 ResNet requires additional fine-tuning of the classification head after model merging. We demonstrate
 1266 that our method still applies to those models.



1282 Figure 10: Pareto front obtained for two ResNet18 models on CIFAR-10 and Flowers-102. We
 1283 perform additional finetuning of the classification head after merging the model weights.

1284

1285

1286

1287

1288

1289

1290

1291

1292

1293

1294

1295

E MORE DETAILS ON ALGORITHMS

E.1 PLAIN LOCMAP

It is important to note that Plain LocMAP (Algorithm 1) is an out-of-the-box plugin-like method. Many parts of it are kept generic: there are multiple ways to sample Ω in terms of the number of \mathbf{c} and the style of sampling (Bayesian or not), thus creating a tradeoff between the quality of the Pareto front and the computational time; the task vector can be computed on the more memory-capable CPU and possibly in a parameter-efficient manner (e.g. LoRA, Adapter, and BiTFiT): for example, computing \mathbf{v}_n via the subtraction of two full 7B models requires $2 \times 23 = 46\text{GB}$ of memory capacity, but the memory cost for PEFT models may reduce to 16MB by only subtracting the non-frozen components; the for-loops in lines 2 and 4 can be computed in parallel, possibly using a much smaller subset of the data, and thus enjoying a computational speed-up.

E.2 NESTED-MERGING LOCMAP

E.2.1 OVERVIEW

In this section, we explain the procedure of the algorithm in Figure 4 in detail.

Empirically, we only need 20 scaling coefficients to get a Pareto front of good quality to merge 2 tasks. However, due to the curse of dimensionality, we need exponentially more pairs of $(\mathbf{c}, \{\tilde{M}_n(\theta_m(\mathbf{c}))\}_{n=1}^N)$ pairs to achieve a good quality of the Pareto front in the case of 8 tasks. Theoretically, in the best case, the number of points required to obtain a good quality Pareto front for N tasks is $O(N^3)$. In the worst case, when the curse of dimensionality dominates, it could be $O(N \cdot 2^N)$. Using the nested merging scheme, we reduce the computation complexity from $O(N \cdot 2^N)$ to $O(N \log_2^N)$. Please refer to Table 8 for the detailed computational complexity comparison. Algorithm details are presented in Algorithm 2.

Algorithm 2 Nested-merging LocMAP

Input: A predetermined preference $pref \in \mathbb{R}^N$ over the N tasks, the tuple of task, loss, task vector:

$$G_n = (\text{task}_n, l_n, \theta_{ft}^n)$$

Normalize $pref$ to make sure the sum is 1

Initialize the set $\tau = \{G_1, \dots, G_N\}$

while $|\tau| > 1$ **do**

Find the pair of $(G_i, G_j) \in \tau$ that are closest to each other in terms of (l_i, l_j)

Implement Algorithm 1 to find the Pareto front $\text{PF}_{i,j}$ between $(\tilde{M}_i, \tilde{M}_j)$

Select $\mathbf{c}^* = (c_i^*, c_j^*) \in \mathbb{R}^2$ based on the Pareto front $\text{PF}_{i,j}$

Merge the models by $\theta_{\text{merge}}^{i,j} = \theta_{\text{pre}} + c_i(\theta_{\text{pre}} - \theta_{ft}^i) + c_j(\theta_{\text{pre}} - \theta_{ft}^j)$

Calculate the weighted average loss on the two tasks $l_{ij} = pref_i l_i + pref_j l_j$

Update τ by replacing $\{G_i, G_j\}$ with $\{G_{ij}\}$, where $G_{ij} \equiv (\text{task}_{i,j}, l_{ij}, \theta_{\text{merge}}^{i,j})$

end

return $\theta_{\text{merge}}^{1,2,\dots,N}$

E.2.2 TIME COMPLEXITY OF NESTED-MERGING LOCMAP

Table 8: Computational cost of model merging for N models.

	# evals per task	minimum # evals (total)	# evals (total)
Naive model merging	$O(N^2)$	$O(N^3)$	$O(N \cdot 2^N)$
Nested model merging	$O(1)$	$O(N \log_2^N)$	$O(N \log_2^N)$

To estimate the computational complexity of nested-merging LocMAP, we denote N as the number of tasks. The number of total evaluations needed for nested-merging LocMAP is: $N/2 \times 2 + \dots + N/2^m \times 2^m = O(N \log_2^N)$ where $2^{m-1} < N \leq 2^m$.

Detailed calculations are as follows. When the number of tasks is 8, in the first rounds, 4 2-task merging procedures are running in parallel. Each of the procedures evaluates 2 tasks. In the procedure of model-merging between 2 tasks, as discussed, we need to sample 20 scaling coefficients \mathbf{c} and evaluate 20 merged models on the 2 tasks. Thus, it takes $4 \times 20 \times 2 = 160$ times of evaluation in the first round. In the second round, 2 2-task merging procedures are running in parallel, each of them evaluating 4 tasks. Thus, it takes $2 \times 20 \times 4 = 160$ times of evaluation. In the last round, there is only one 2-task merging and evaluation on 8 tasks. It takes $1 \times 20 \times 8 = 160$ times of evaluation. In total, NMLocMAP takes 480 times of evaluations. Generalizing the calculation, the number of rounds can be calculated by $\log_2(N)$. In each round, we need to evaluate $T \cdot N/2^i \cdot 2^i = TN$ where T is the number of scaling coefficient vectors needed to be evaluated when the number of tasks is 2. In the above example, $T = 20$. Thus, the time complexity is $O(TN \log_2(N))$. We rewrite it as $O(N \log_2(N))$ if ignoring T which is a constant.

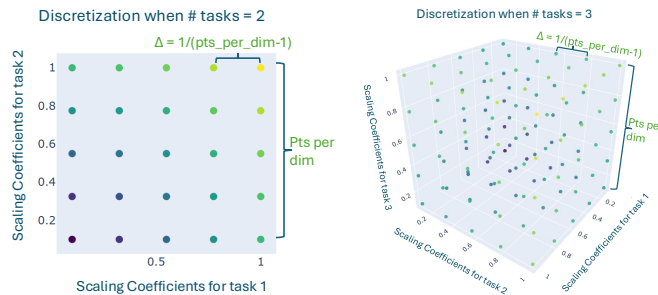


Figure 11: The discretization of scaling coefficients when the number of tasks is 2 and 3. As the dimension grows, preserving the same number of pts per dimension results in exponentially more grid points. This serves to illustrate why when the dimension is low (e.g., < 4), we can regard the brute-force direct search method as ground truth, but it becomes insufficient when the dimension is higher.

E.2.3 INTERMEDIATE PARETO FRONTS IN EACH ROUND

To determine if NMLocMAP affects performance negatively when compared to merging multiple models in a single operation. We show the intermediate Pareto fronts obtained when merging 8 models using nested-merging LocMAP in Figure 12, where we merge two models at a time. The figures illustrate the intermediate Pareto fronts obtained, where A_B means the model obtained by merging model A and model B.

1404
 1405
 1406
 1407
 1408
 1409
 1410
 1411
 1412
 1413
 1414
 1415
 1416
 1417
 1418
 1419
 1420
 1421
 1422
 1423
 1424
 1425
 1426
 1427
 1428
 1429
 1430
 1431
 1432
 1433
 1434
 1435
 1436
 1437
 1438
 1439
 1440
 1441
 1442
 1443
 1444
 1445
 1446
 1447
 1448
 1449
 1450
 1451
 1452
 1453
 1454
 1455
 1456
 1457

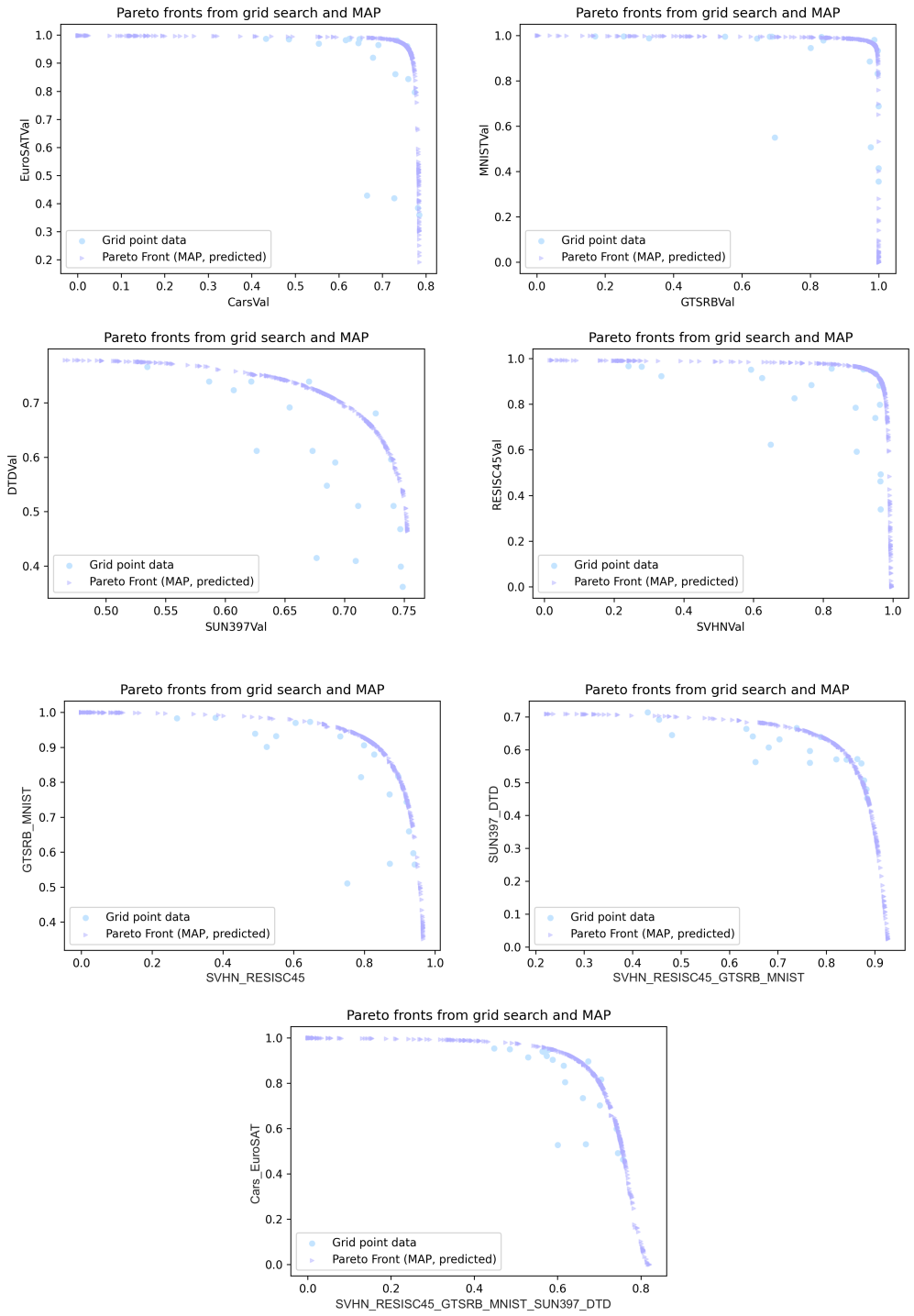


Figure 12: Illustration of the sequential steps involved in merging 8 models using nested-merging LocMAP (left to right, top to bottom). The figures show the intermediate Pareto fronts obtained, where A_B means the model obtained by merging model A and model B.

E.2.4 RESULTS ON USING NESTED MERGING TO MERGE 8 MODELS

We further evaluate the effectiveness of nested-merging LocMAP. Supplemental Figure 12 shows the intermediate Pareto fronts obtained using nested-merging LocMAP (NMLocMAP) sequentially.

Table 9: We compared nested-merging LocMAP with LocMAP and baseline methods in merging 8 models using a set of 10 preference vectors in terms of preference-weighted sum of accuracies.

Metric	Single-task models	LocMAP-nested	LocMAP-plain	TIES-merging	DARE-TIES	Task Arithmetic (TA)	DARE-TA
Preference weighted sum (\uparrow)	90.05 \pm 3.02	67.05 \pm 3.89	72.12 \pm 3.78	70.79 \pm 3.81	70.51 \pm 3.58	59.44 \pm 5.68	63.14 \pm 4.91

In addition, we compared the performance of NMLocMAP with Plain LocMAP (Algorithm 1). The results are shown in Table 9. The results confirm that nested-merging LocMAP can obtain comparable results to those obtained by LocMAP while using much fewer evaluation runs. As discussed in Appendix E.2.2, in total, we run $40 \times 4 + 80 \times 2 + 160 \times 1 = 480$ evaluations. In contrast, when running the Plain LocMAP (Algorithm 1), we used 280 coefficients and evaluate $280 \times 8 = 2240$ times. In addition, while being suboptimal to LocMAP (Algorithm 1), nested-merging LocMAP can still outperform other baseline methods such as TA and DARE-TA in accommodating various user preferences with relatively low computational cost, especially when the number of tasks is high.

E.3 BAYESIAN LOCMAP

Figure 13 includes illustration of our discretization method (how we create bins) in 2D and 3D decision variable (\mathbf{c}) space.

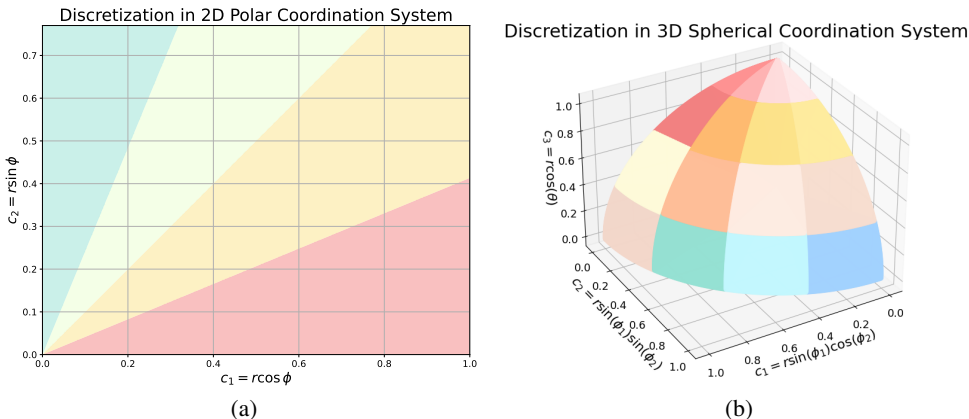


Figure 13: (a) Discretizing of two task scaling coefficients along the angular dimension in 2D polar coordinate system; (b) Discretizing of three task scaling coefficients along the angular dimensions in 3D spherical coordinate system;

E.3.1 PERFORMANCE OF BAYESIAN LOCMAP

We further improve the efficiency of LocMAP by proposing an adaptive Bayesian sampling algorithm. This Bayesian approach samples the points from regions with the highest level of uncertainty, where uncertainty is quantified with the Upper Confidence Bound (UCB). Please refer to Algorithm 3 for more details about the algorithm.

Please refer to Figure 14 for the experimental results comparing Bayesian LocMAP Algorithm 3 with LocMAP Algorithm 1. The very left column shows the names of the 2 tasks being merged. Below, we define points (pts) as scaling coefficients and evaluation metrics of the corresponding merged models. Please note that the results shown in this figure are the mean of 7 merging tasks that merge 2 models: DTD+Cars, DTD+RESISC45, EuroSAT+RESISC45, GTSRB+Cars, GTSRB+RESISC45, RESISC45+SVHN, SUN397+SVHN. The Pareto front estimated by Bayesian LocMAP with only one iteration (6+3 pts) is shown in Figure 15.

The experiments are initialized with 6 pairs of \mathbf{c} , $\{M_n\}_{n=1}^N$ (iter 0). In every following iteration, we sample more points following the Bayesian adaptive sampling algorithm. We compare the Bayesian

Algorithm 3 Bayesian Adaptive of Surrogate Model

Input: Number of iterations J , Buffer \mathcal{B} , Pretrained model θ_{pre} , Task vectors \mathbf{v}_n , Evaluators for task N , $M_n(\cdot)$, Discretization bin number K , sample size for every iteration n_j , $j = 0$ to J , Bootstrap dropping rate $\alpha = 20\%$, Bootstrap sampling number $Q = 30$.

```

1512  $\mathcal{B} \leftarrow \emptyset$ 
1513 for  $j = 0$  to  $J$  do
1514   if  $j = 0$  then
1515     | Sample  $n_0$  scaling coefficients  $\{\mathbf{c}_i\}_{i=1}^{n_j}$  from  $U([0, 1]^N)$ 
1516   else
1517     | Sample  $n_j$  scaling coefficients  $\{\mathbf{c}_i\}_{i=1}^{n_j}$  based on the posterior distribution
1518   end
1519   for  $i = 0$  to  $n_j$  do
1520     | Merge the model  $\theta_m(\mathbf{c}_i) = \theta_{\text{pre}} + \mathbf{c}_i \cdot \mathbf{v}_n$  Evaluate  $m_{n,i} = M_n(\theta_m(\mathbf{c}_i))$   $\mathcal{B} \leftarrow \mathcal{B} \cup \{(\mathbf{c}_i, m_{n,i})\}$ 
1521   end
1522   Fit the quadratic approximation surrogate model  $\tilde{M}_n$  by learning  $\mathbf{A}_n^*$ ,  $\mathbf{b}_n^*$ ,  $e_n^*$  in Equation (5).
1523   Discretize the scaling coefficients along the angular dimensions in hyper-spherical coordinates
1524   (see Figure 13 as examples)
1525   for  $k = 0$  to  $K$  do
1526     | Calculate the mean of  $L2$  loss between  $\tilde{M}_n(\mathbf{c}_i)$  and  $M_t(\mathbf{c}_i)$ , where  $\mathbf{c}_i$  are in bin  $k$ , denoted
1527     | as  $\text{mean}_k$ 
1528     | Bootstrap to estimate the standard deviation of the losses.
1529     | for  $q = 0$  to  $Q$  do
1530     |   | Randomly (uniformly) drop  $\alpha$  scaling coefficient in bin  $k$  Calculate the mean of  $L2$  loss
1531     |   | between  $\tilde{M}_n(\mathbf{c}_i)$  and  $M_t(\mathbf{c}_i)$  with the rest points and denoted with  $l_q$ 
1532     |   end
1533     |   Calculate the standard deviation of the  $\{l_q\}_{q=0}^Q$  and denoted as  $\text{std}_k$   $\text{score}_k = \text{mean}_k + \frac{1}{2}\text{std}_k$ 
1534     | end
1535     Calculate probability distribution across the discretized bins by  $\text{score}_k$  as the posterior sampling
1536     strategy in the next round
1537   end
1538 end

```

adaptive sampling beginning with 6 points and adding 3 additional points (6 + 3 pts) with running Algorithm 1 with 9 points in a row. We also compare the Bayesian adaptive sampling beginning with 6 points and adding 3 additional points for 2 times (6 + 2 × 3 pts) with running Algorithm 1 with 12 points in a row. We show that, in most cases, utilizing the same number of points, Bayesian adaptive sampling performs better than the run-in-a-row scheme in Algorithm 1.

In conclusion, when the number of data points (scaling coefficients and evaluation metrics of the corresponding merged models) is small, Bayesian LocMAP Algorithm 3 performs better than LocMAP Algorithm 1. As the number of data points increases, their performance becomes closer. Thus, we recommend implementing Bayesian LocMAP when computational resources are very limited and the number of models (tasks) to merge is not high.

1566
 1567
 1568
 1569
 1570
 1571
 1572
 1573
 1574
 1575
 1576
 1577
 1578
 1579
 1580
 1581
 1582
 1583
 1584
 1585
 1586
 1587
 1588
 1589
 1590
 1591
 1592
 1593
 1594
 1595
 1596
 1597
 1598
 1599
 1600
 1601
 1602
 1603
 1604
 1605
 1606
 1607
 1608
 1609
 1610
 1611
 1612
 1613
 1614
 1615
 1616
 1617
 1618
 1619

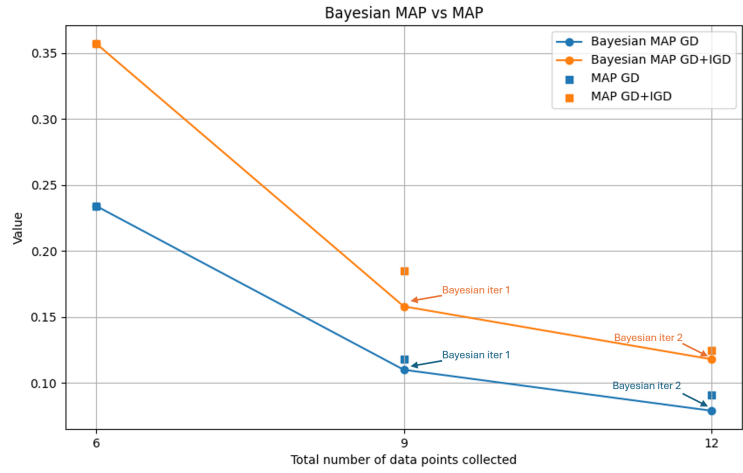


Figure 14: Bayesian LocMAP compared to LocMAP. The x-axis represents the number of points used by either LocMAP or Bayesian LocMAP, while the y-axis represents the value for IGD or GD. We compared LocMAP with 6, 9, and 12 points, and Bayesian LocMAP with 6 initial points, sampling 3 more points each round for two rounds.

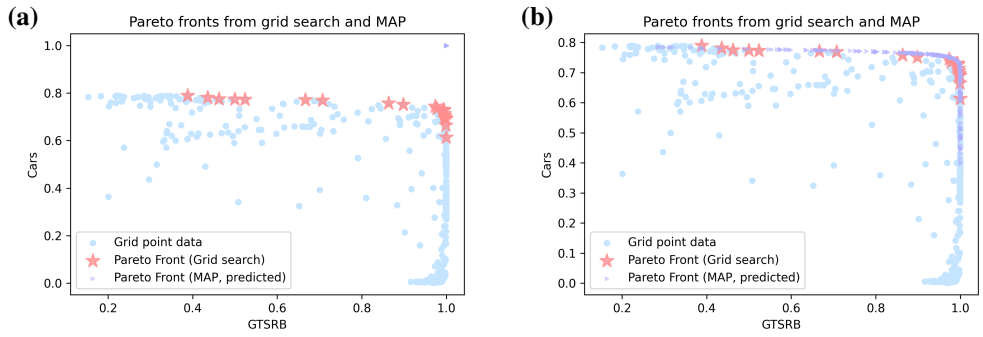


Figure 15: (a) This plot shows a failure case of the amortized Pareto front when we only have 6 initial randomly sampled pairs of $(\mathbf{c}, \{M_i(\theta_m(\mathbf{c}))\}_{i=1}^N)$ (b) After one iteration of Bayesian adaptive sampling for 3 more pairs (9 in total), the amortized Pareto front is much better than the initial Pareto front.

1620 F POTENTIAL Q & A

1621 In this section, we anticipate and address some potential questions that readers might have.

1622 F.1 THE AUTHORS ASSUME A SETTING WHERE IT IS COMPUTATIONALLY EXPENSIVE TO 1623 QUERY THE MODEL EVALUATIONS. BUT IS THIS THE REALITY?

1624 Yes, to get the Pareto front of tasks that have trade-offs. We need to have a lot of data points to show
1625 the trade-off. Here, each data point is the evaluation metric of a model. To get the ground truth
1626 evaluation metric of a task (e.g. let’s say classification), we need to run the evaluation script of the
1627 model to determine the metric. If we have 4 tasks, and we set 5 possible values (let’s say 0.2, 0.4,
1628 0.6, 0.8, 1) for the scaling coefficient vector of each model specialized for one task. We will have to
1629 evaluate $5^4 = 625$ models on all 4 tasks. Assuming each evaluation takes 1 minute, evaluating all the
1630 models on all the 4 tasks will take $625 \text{ models} \times 4 \text{ tasks} \times 1 \text{ minute} = 2500 \text{ minutes} = 41.7 \text{ hours}$
1631 which is expensive. In big O notation, assuming we have T tasks, the time of evaluation for each task
1632 is T . The time (computational) complexity is $O(TN2^N)$.

1633 F.2 HOW IS LOCMAP DIFFERENT FROM OTHER MOOP METHODS, SUCH AS LINEAR 1634 SCALARIZATION?

1635 **Computational Efficiency** LocMAP is computationally efficient because it leverages a surrogate
1636 model (the quadratic approximation) to estimate the evaluation metrics for different model com-
1637 binations. Once the quadratic model is learned, solving the optimization problem (approximating
1638 the Pareto front) is much faster because the complexity is reduced to optimizing over the quadratic
1639 approximation, rather than needing to directly evaluate the task metrics over the entire solution space.

1640 Additionally, LocMAP doesn’t require gradient descent or re-training when merging models and the
1641 surrogate model provides an efficient way to approximate the Pareto front without re-evaluating every
1642 model configuration.

1643 On the other hand, linear scalarization involves computing a weighted sum of the objectives and
1644 solving it as a single-objective optimization problem. However, it often requires multiple optimization
1645 runs with different weight configurations to explore different points on the Pareto front. Since linear
1646 scalarization doesn’t model non-linear relationships, it might require more iterations or grid searches
1647 over different weights to achieve a decent approximation of the Pareto front. This can become
1648 computationally expensive, especially for a large number of tasks or highly complex models.

1649 **Non-convex Pareto Fronts** Many real-world multi-objective optimization problems have non-
1650 convex Pareto fronts, which require more sophisticated methods. While linear scalarization can only
1651 explore the convex regions of the Pareto front, NSGA-III allows LocMAP to discover non-convex
1652 regions of the Pareto front. It does this by evolving a population of solutions that are non-dominated
1653 (i.e., not Pareto dominated by any other solution) and spreading these solutions across the entire
1654 Pareto front, including both convex and non-convex regions.

1655 F.3 WHY DOES QUADRATIC APPROXIMATION HAVE A LOWER COST?

1656 For the LocMAP algorithm (Algorithm 1), the time complexity is the same as what we mentioned
1657 above; what is different is that we fitted an approximation of the evaluation metrics. We only need
1658 the scaling coefficient vectors to input to a quadratic function model to be able to get the estimated
1659 evaluation score. Running the quadratic function once takes only $3.91 \times 10^{-6} s \pm 894 \times 10^{-9} s$. Thus,
1660 evaluating 2500 times takes $< 2500 \times 4 \times 10^{-6} s = 10^{-2} s$.

1661 F.4 WHY NOT COMPARE TO GIT-REBASIN AINSWORTH ET AL. (2023)?

1662 We didn’t compare our method to Git Re-Basin because their study focuses on the scenarios of
1663 merging the models from different initializations, whereas our background works on the same
1664 initialization of different fine-tuned models.

1674 F.5 WHY DOES NESTED-MERGING LOCMAP NOT GIVE A COMPLETE PARETO FRONT?
1675

1676 In nested-merging LocMAP, we merge the models in pairs. For example, there are $model_i$ for task i
1677 as individual fine-tuned models where $i = 1, 2, 3, 4$. We first merge model 1 and model 2 given the
1678 preference of the user between task 1 and task 2. We then get $model_{1,2}$. At the same time, we merge
1679 model 3 and model 4 given the preference of the user between task 3 and task 4 and get $model_{3,4}$.
1680 Finally, we merge the $model_{1,2}$ and $model_{3,4}$ given the preference of user to get $model_{1,2,3,4}$. We
1681 output the $model_{1,2,3,4}$ as the output merged model of the algorithm. Please note that the merging
1682 order in the algorithm should be decided by the loss function clustering. It is a heuristic decision and
1683 does not always dominate other merging orders. Thus, we choose not to emphasize the contribution
1684 of this order. The practitioner may use any order they think can be helpful for the merging.

1685 F.6 IT SEEMS NESTED-MERGING LOCMAP PERFORMS WORSE THAN LOCMAP. WHAT IS THE
1686 MEANING OF IT?
1687

1688 In theory, the surrogate model can be easily fitted when the number of tasks is low. When it is
1689 high (e.g. 8), the fit of the surrogate model can no longer be a near-perfect approximation (please
1690 find the R^2 in Table 3). Thus, even if the NMLocMAP can only find the suboptimal solution, it
1691 is still comparable to LocMAP Algorithm 1 according to Table 9. We understand in general that
1692 NMLocMAP does not find the global optimum, but please kindly keep in mind that even if their
1693 performance is comparable, NMLocMAP takes way less computation for evaluation.
1694

1695 F.7 WHY DOES NESTED-MERGING LOCMAP NOT OUTPUT THE OPTIMAL SOLUTION?
1696

1697 The solution found by nested-merging LocMAP (NMLocMAP) is indeed suboptimal given the
1698 limited search space compared with merging all models at once. However, it does not mean that it
1699 is not useful in all situations. When the number of tasks is high, it has comparable performance to
1700 LocMAP while consuming much fewer computations for evaluation.
1701

1702 F.8 HOW DO YOU DEAL WITH GRADIENT AND HESSIAN IN THE SECOND-ORDER TAYLOR
1703 EXPANSION?
1704

1705 Notations:

- 1706 • p as the number of parameters in the pre-trained model (also the number of parameters in
1707 each task vector).
- 1708 • \mathbf{V} is the matrix of task vectors of different N tasks. Thus, $\mathbf{V} \in \mathbb{R}^{p \times N}$.
- 1709 • \mathbf{c} is the scaling coefficient vector $\in \mathbb{R}^N$.
- 1710 • M_n is the metric (e.g. accuracy) for the task n .

$$1711 M_n(\mathbf{c}) = \underbrace{M_n(\boldsymbol{\theta}_{\text{pre}})}_{\in \mathbb{R}} + \underbrace{\nabla M_n(\boldsymbol{\theta}_{\text{pre}})}_{\in \mathbb{R}^{1 \times p}}^\top \underbrace{\mathbf{V}}_{\in \mathbb{R}^{p \times N}} \underbrace{\mathbf{c}}_{\in \mathbb{R}^{N \times 1}} + \frac{1}{2} \underbrace{(\mathbf{V}\mathbf{c})^\top}_{\in \mathbb{R}^{1 \times p}} \underbrace{\mathbf{H}_n(\boldsymbol{\theta}_{\text{pre}})}_{\in \mathbb{R}^{p \times p}} \underbrace{\mathbf{V}\mathbf{c}}_{\in \mathbb{R}^{p \times 1}} + \underbrace{R_n}_{\in \mathbb{R}} \quad (6)$$

$$1712 = \underbrace{e_n}_{\in \mathbb{R}} + \underbrace{\mathbf{b}_n^\top}_{\in \mathbb{R}^{1 \times N}} \underbrace{\mathbf{c}}_{\in \mathbb{R}^{N \times 1}} + \underbrace{\mathbf{c}^\top}_{\in \mathbb{R}^{1 \times N}} \underbrace{\mathbf{A}_n}_{\in \mathbb{R}^{N \times N}} \underbrace{\mathbf{c}}_{\in \mathbb{R}^{N \times 1}} \quad (7)$$

1713 (8)

$$1714 \tilde{M}_n(\mathbf{c}; \mathbf{A}_n, \mathbf{b}_n, e_n) \equiv e_n + \mathbf{b}_n^\top \mathbf{c} + \frac{1}{2} \mathbf{c}^\top \mathbf{A}_n \mathbf{c}$$

1715 where

$$1716 \mathbf{A}_n = \mathbf{V}^\top \mathbf{H}_n(\boldsymbol{\theta}_{\text{pre}}) \mathbf{V} \in \mathbb{R}^{N \times N}, \mathbf{b}_n = \mathbf{V}^\top \nabla M_n(\boldsymbol{\theta}_{\text{pre}}) \in \mathbb{R}^N, e_n = M_n(\boldsymbol{\theta}_{\text{pre}}) + R_n \quad (9)$$

1728 Please notice that \mathbf{A} is a symmetric matrix. Specifically, when the number of tasks is 2, we have:

1729
1730
$$\tilde{M}_1(\mathbf{c}; \mathbf{A}_1, \mathbf{b}_1, e_1) \equiv e_1 + \mathbf{b}_1^\top \mathbf{c} + \frac{1}{2} \mathbf{c}^\top \mathbf{A}_1 \mathbf{c} \quad (10)$$

1731
1732
$$= \frac{1}{2} A_{1,11} c_1^2 + A_{1,12} c_1 c_2 + \frac{1}{2} A_{1,22} c_2^2 + b_{1,1} c_1 + b_{1,2} c_2 + e_1 \quad (11)$$

1733
1734
$$\tilde{M}_2(\mathbf{c}; \mathbf{A}_2, \mathbf{b}_2, e_2) \equiv e_2 + \mathbf{b}_2^\top \mathbf{c} + \frac{1}{2} \mathbf{c}^\top \mathbf{A}_2 \mathbf{c} \quad (12)$$

1735
1736
$$= \frac{1}{2} A_{2,11} c_1^2 + A_{2,12} c_1 c_2 + \frac{1}{2} A_{2,22} c_2^2 + b_{2,1} c_1 + b_{2,2} c_2 + e_2 \quad (13)$$

1737
1738
$$(14)$$

1739
1740 We don't calculate the gradient or Hessian to get \mathbf{A}_1 , \mathbf{A}_2 , \mathbf{b}_1 , \mathbf{b}_2 , e_1 and e_2 . We use linear regression
1741 to estimate them. How? Given a (c_1, c_2) pair, we can define a merged model $\theta_{\text{merge}}(c_1, c_2)$. We
1742 evaluate the merged model on task 1 and task 2 to get the metrics (e.g. accuracy). Given 20 pairs
1743 of (c_1, c_2) , we would be able to evaluate and get 20 corresponding, (M_1, M_2) which are metrics for
1744 task 1 and task 2. Thus, we can fit the surrogate model $\tilde{M}_1(\mathbf{c}; \mathbf{A}_1, \mathbf{b}_1, e_1)$ and $\tilde{M}_2(\mathbf{c}; \mathbf{A}_2, \mathbf{b}_2, e_2)$.

1745
1746
1747
1748
1749
1750
1751
1752
1753
1754
1755
1756
1757
1758
1759
1760
1761
1762
1763
1764
1765
1766
1767
1768
1769
1770
1771
1772
1773
1774
1775
1776
1777
1778
1779
1780
1781